© 2017. Published by The Company of Biologists Ltd | Development (2017) 144, 115-127 doi:10.1242/dev.143131

RESEARCH ARTICLE

Interactions between mural cells and endothelial cells stabilize the developing zebrafish dorsal aorta

Amber N. Stratman[1], Sofia A. Pezoa[1,*], Olivia M. Farrelly[1,*], Daniel Castranova[1,*], Louis E. Dye III[2], Matthew G. Butler[1], Harwin Sidik[3], William S. Talbot[3] and Brant M. Weinstein[1,‡]

ABSTRACT

Mural cells (vascular smooth muscle cells and pericytes) play an essential role in the development of the vasculature, promoting vascular quiescence and long-term vessel stabilization through their interactions with endothelial cells. However, the mechanistic details of how mural cells stabilize vessels are not fully understood. We have examined the emergence and functional role of mural cells investing the dorsal aorta during early development using the zebrafish. Consistent with previous literature, our data suggest that cells ensheathing the dorsal aorta emerge from a sub-population of cells in the adjacent sclerotome. Inhibition of mural cell recruitment to the dorsal aorta through disruption of *pdgfr* signaling leads to a reduced vascular basement membrane, which in turn results in enhanced dorsal aorta vessel elasticity and failure to restrict aortic diameter. Our results provide direct *in vivo* evidence for a functional role for mural cells in patterning and stabilization of the early vasculature through production and maintenance of the vascular basement membrane to prevent abnormal aortic expansion and elasticity.

KEY WORDS: Vascular smooth muscle, Pericyte, Zebrafish, PDGFR signaling, Vascular basement membrane

INTRODUCTION

Mural cells – vascular smooth muscle cells (vSMCs) and pericytes – play crucial roles in establishment and long-term stabilization of blood vessels (Bergers and Song, 2005; Abraham et al., 2008; Owens, 1995; Armulik et al., 2011a; Jain, 2003). vSMCs are recruited to large-caliber vessels, namely arteries, arterioles and veins, where they concentrically wrap the endothelium, fully encasing the vessels in multi-layered smooth muscle sheaths. Interactions between endothelial cells (ECs) and vSMCs are thought to strengthen the maturing vascular wall to increases in flow and shear stress while helping to regulate vessel contractility and tone. Pericytes are associated with smaller-caliber vessels, in particular capillary beds and post-capillary venules. Pericytes associate with these smaller-caliber vessels in lower numbers, with pericyte/EC ratios between 1:1 and 1:10, localizing primarily along endothelial cell-cell junctions, branch points, and in areas that need to maintain high levels of barrier function [such as the blood-brain barrier (BBB)] (Ando et al., 2016; Owens, 1995; Daneman et al., 2010; Armulik et al., 2010, 2011a,b). PDGF-BB/PDGFRβ signaling is required for recruitment of vSMCs and pericytes to vessels (Hellstrom et al., 1999; Fortuna et al., 2015; Lindblom et al., 2003; Lindahl et al., 1997; Hirschi et al., 1999; Lehti et al., 2005; Benjamin et al., 1998), although a variety of other signaling pathways have been shown to contribute to mural cell differentiation, recruitment and stabilization, in particular TGFβ, Notch and EGF signaling among others (Lee et al., 2007; Higashiyama et al., 1993; Iivanainen et al., 2003; Krymskaya et al., 1997; Wang et al., 2014, 2012; Kofler et al., 2015; Fortuna et al., 2015; Kennard et al., 2008; Hirschi et al., 2003; Aplin et al., 2010; Stratman et al., 2010; Zaucker et al., 2013).

Mouse lineage tracing and chick/quail chimera studies have led to the adoption of a multi-site hypothesis for the ontogeny of mural cells (reviewed in Majesky, 2007; Pouget et al., 2008; Wiegreffe et al., 2007; Wasteson et al., 2008; Armulik et al., 2011a). In summary, vSMCs in the head and central nervous system appear to be derived from the neural crest, while smooth muscle cells in the gut, liver and lung seem to be of mesothelial origin. The developmental origins of mural cells investing the dorsal aorta are less well described, with at least two main sites proposed based on chick, mouse and zebrafish data as possible contributors of aortic vSMCs: the neural crest and the sclerotome/somite. In general, all studied models of vSMC ontogeny suggest an epithelial to mesenchymal transition (EMT) for mesothelial cells as they delaminate and then migrate to various anatomical locations.

EC-mural cell interactions have been implicated in production and maintenance of the vascular basement membrane to help promote blood vessel stabilization and quiescence (Jain, 2003; Davis and Senger, 2005; Hynes, 2007). EC-pericyte co-culture assays *in vitro* and quail chick chorioallantoic membrane (CAM) assays have provided evidence that pericytes help to maintain extracellularly deposited basement membrane proteins (Stratman and Davis, 2012; Stratman et al., 2009, 2010; Zhao et al., 2015). Although ECs appear to have the capacity to synthesize basement membrane proteins on their own, they do not appear to be properly deposited to form an EC-associated basement membrane in the absence of mural cells, or mural cells/astrocytes in the case of the BBB (Abraham et al., 2008; Armulik et al., 2010, 2011b; Yao et al., 2014; Chen et al., 2013). Although these assays suggest that EC-mural cell interactions are important for building and maintaining the vascular basement membrane, a full analysis of the requirement for both cell types in formation and stabilization of the basement membrane in the developing vasculature of an intact organism, in particular around larger-caliber vessels such as the dorsal aorta, has not been carried out.

Here, we show data suggesting that vSMCs associated with the dorsal aorta are derived from a sub-population of the sclerotome,

[1]Program in Genomics of Differentiation, National Institute of Child Health and Human Development, National Institutes of Health, Bethesda, MD 20892, USA. [2]Microscopy & Imaging Core, National Institute of Child Health and Human Development, National Institutes of Health, Bethesda, MD 20892, USA. [3]Department of Developmental Biology, Stanford University School of Medicine, Stanford, CA 94305, USA.
*These authors contributed equally to this work

‡Author for correspondence (flyingfish2@nih.gov)

B.M.W., 0000-0003-4136-4962

Received 1 August 2016; Accepted 17 November 2016

Development (2017) 144, 115-127 doi:10.1242/dev.143131

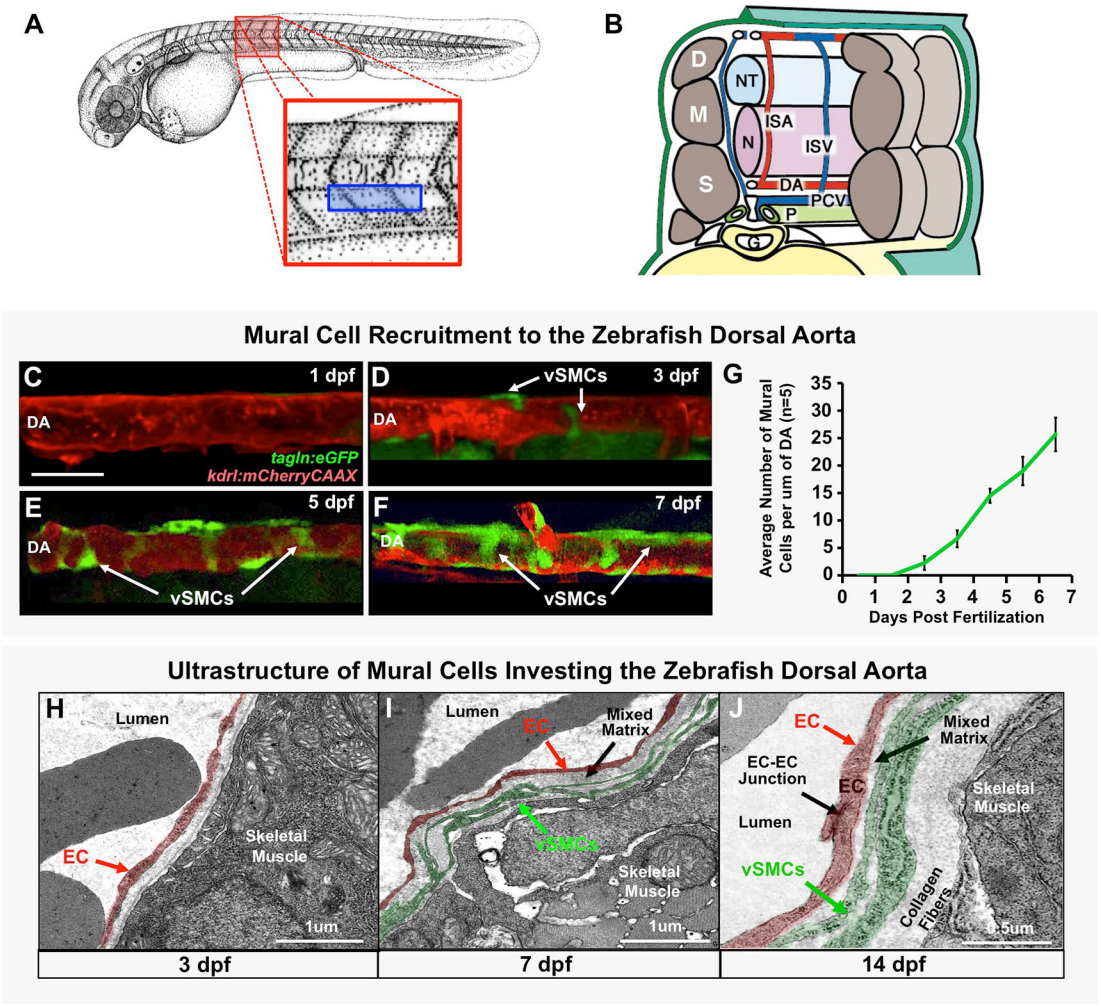

Fig. 1. Vascular smooth muscle cells associate with the zebrafish dorsal aorta. (A) Camera lucida drawing of a 2 dpf zebrafish embryo (Kimmel et al., 1995), with the magnified red boxed region shown in B and blue boxed region imaged in C-F. (B) Schematic ('cut-away') diagram showing the anatomy of the zebrafish trunk and its blood vessels at approximately 2 days post-fertilization. Trunk circulation flows through the dorsal aorta (DA), posterior cardinal vein (PCV) and intersegmental arteries (ISA) and intersegmental veins (ISV). The vessels are shown relative to adjacent tissues and structures in the mid-trunk including the gut (G), notochord (N), neural tube (NT), left pronephric duct (P), dermamyotomes (D), myotomes (M) and sclerotomes (S). (C-F) Representative confocal images of the dorsal aorta in *Tg(tagln:egfp), Tg(kdrl:mCherryCAAX)* double transgenic zebrafish at 1 dpf (C), 3 dpf (D), 5 dpf (E), or 7 dpf (F), with red fluorescent vascular endothelium and green fluorescent vSMCs, showing accumulation of vSMCs on the dorsal aorta. (G) Quantification of vSMC accumulation on the first 6-somite segments of the dorsal aorta at 1-7 dpf. Values are mean±s.e.m.; *n*=5 fish. (H-J) Vascular smooth muscle cell investment of the DA was confirmed by electron microscopy. Representative images of the dorsal aorta wall at 3 dpf (H), 7 dpf (I) and 14 dpf (J) are shown. ECs and vSMCs are pseudo-colored red and green, respectively. Panel B is adapted from Isogai et al. (2003). Scale bar: 50 µm (C-F).

and further demonstrate that recruitment of vSMCs to the dorsal aorta in the fish is dependent on PDGFRβ signaling. Reduced vSMC recruitment to the dorsal aorta following disrupted PDGFRβ signaling leads to decreased aortic accumulation of basement membrane proteins, along with increased aortic diameter and increased aortic wall elasticity. These data show that mural cell recruitment to the developing aorta is essential for proper assembly and maintenance of the developing vascular wall *in vivo*.

RESULTS

Mural cells invest the dorsal aorta in the developing zebrafish

The dorsal aorta is the major trunk axial artery, and is one of the first vessels to assemble during early development in all vertebrates. The dorsal aorta forms immediately below the notochord and immediately above the posterior cardinal vein, the major trunk axial vein (Fig. 1A,B). In mammals, the dorsal aorta becomes heavily invested with supporting vSMCs beginning early in embryogenesis (Owens, 1995; Armulik et al., 2011a).

We used the experimentally accessible, optically clear zebrafish embryo to study the ontogeny of smooth muscle (mural) cells contributing to the wall of the dorsal aorta. A number of previous studies have provided solid documentation that the zebrafish dorsal aorta acquires a vSMC-containing vascular wall similar to that found in other vertebrates, and have suggested a somitic origin for these cells (Santoro et al., 2009; Whitesell et al., 2014; Fortuna et al., 2015; Wang et al., 2014; Ando et al., 2016; Zaucker et al., 2013). We crossed a previously reported zebrafish *Tg(tagln:egfp)* smooth muscle cell transgenic reporter line (Seiler et al., 2010; Yang et al., 2003) to a *Tg(kdrl:mCherryCAAX)* red fluorescent vascular endothelial-specific transgenic reporter line (Fujita et al., 2011) and employed confocal microscopy to examine the time course of mural/vSMC recruitment to the dorsal aorta during early

Development (2017) 144, 115-127 doi:10.1242/dev.143131

development (Fig. 1C-G, Fig. S1). At 1 day post-fertilization (dpf) no vSMCs are observed along the mid-trunk dorsal aorta (Fig. 1C), but by 3 dpf, a small number of GFP-positive vSMCs are clearly associated with this vessel (Fig. 1D). Dorsal aorta-associated vSMCs continue to increase in number and begin to wrap around the vessel at the 5 dpf and 7 dpf time points (Fig. 1E-G). Rostral portions of the dorsal aorta become invested with vSMCs earlier than more caudal portions of the dorsal aorta (Fig. S2A-E). vSMC investment of the trunk intersegmental vessels lags behind that of the dorsal aorta, while the posterior cardinal vein lags even further behind (Fig. S2F-I).

We used electron microscopy (EM) to show that dorsal aorta-associated GFP-positive cells represent bona fide perivascular mural cells. *Tg*(*tagln:egfp)* transgenic animals and *Tg(kdrl:egfp)* controls were collected separately at 3, 7 and 14 dpf and processed for conventional transmission EM and immuno-EM. Representative TEM images at 3, 7 and 14 dpf are shown with the endothelium pseudocolored red and vSMCs pseudocolored green (Fig. 1H-J). The identity of these cells was evident from their anatomical location and morphological features, but more directly confirmed by immuno-EM. Anti-GFP immuno-EM showed that the presumptive endothelium of the dorsal aorta was labeled with nano-gold particles in samples from *Tg(kdrl:egfp)* fish, while presumptive vSMCs were labeled in samples from *Tg(tagln:egfp)* animals (Fig. S3). Our EM results also confirmed that there are few vSMCs associated with the dorsal aorta at 3 dpf (Fig. 1H), but that these cells accumulate in number by 7 dpf (Fig. 1I), and even more so by 14 dpf (Fig. 1J), at which time a few tightly associated vSMC layers are apparent along the length of the dorsal aorta that resemble those found on developing arteries of other vertebrates (Whitesell et al., 2014; Hellstrom et al., 1999; Santoro et al., 2009).

Various sites of origin have been proposed for the progenitors of vSMCs in the trunk, including the somites and the neural crest (Fig. 2A,B), with recent work in the zebrafish and other species suggesting that the majority of trunk vSMCs are mesothelial derived (Ando et al., 2016; Majesky, 2007; Pouget et al., 2008; Wiegreffe et al., 2007; Wasteson et al., 2008; Armulik et al., 2011a). Prior to the onset of vSMC recruitment to the dorsal aorta, vSMC markers *tagln* (*sm22*) and *pdgfrb* are expressed fairly broadly in the ventral-medial quadrant of the somites (Fig. 2C,D), with the highest expression concentrated in *twist1a*-positive sclerotome adjacent to the dorsal aorta (Fig. 2E). By 3 dpf, trunk expression of *tagln* and *pdgfrb* is restricted mainly to presumptive SMCs localized on or near the dorsal aorta and the developing gut (Fig. 2F,G), with *twist1a* expression also largely restricted to the vicinity of the dorsal aorta (Fig. 2H), consistent with a possible sclerotomal origin for dorsal aorta vSMCs.

To rule out neural crest as a source of mural cell progenitors (Fig. 2B), we examined the offspring of *Tg(sox10:rfp);Tg*(*tagln:egfp)* double-transgenic animals (Fig. 2I). Previous reports have documented *Tg(sox10:rfp)* transgene expression in both pre-migratory neural crest and neural crest-derived cells (Kucenas et al., 2008), and examination of double transgenic animals showed that, as previously described, the *Tg(sox10:RFP)* transgene was strongly expressed in the neural tube and neural crest (Fig. 2I). Although we could also easily detect green fluorescent *Tg(tagln:egfp)* transgene-positive cells along the dorsal aorta at 3.5 dpf, none of these cells were red fluorescent (Fig. 2I), confirming that this population of vSMCs was not of neural crest origin.

To examine whether the sclerotome serves as a source of aortic vSMCs, we utilized a previously reported zebrafish *Tg*(*ola-twist1:gal4)* transgenic line with a medaka Twist1 promoter (ola-twist1) expressing Gal4 in the sclerotome (Lee et al., 2013; Yasutake et al., 2004; Yeo et al., 2009; Germanguz et al., 2007) to drive expression of a *UAS:kaede* transgene (Fig. 2J). Examination of the progeny of double transgenic *Tg*(*ola-twist1:gal4); Tg(UAS:kaede)* animals or triple transgenic *Tg*(*ola-twist1:gal4); Tg(UAS:kaede); Tg(kdrl:mCherryCAAX)* animals showed that the sclerotome was indeed expressing kaede at early time points (Fig. S4A) and at later time points *twist1*-positive cells were observed along the dorsal aorta (Fig. S4B,C). We crossed *Tg*(*ola-twist1:gal4);Tg(UAS:kaede)* double transgenics to the *Tg(tagln:nls-egfp-2a-cfp-f)*^{y450} line, photoconverted the sclerotomally expressed kaede to red fluorescence at 4 dpf, and then examined the mural cell coverage of the dorsal aorta of photoconverted animals. We found that most GFP-positive vSMC nuclei on the dorsal aorta overlapped with cells containing photoconverted *twist1*-driven red kaede (Fig. 2K, arrowheads), consistent with a sclerotomal origin for these cells.

To examine more directly whether sclerotome-derived cells contribute to aortic vSMCs (Fig. 2A), we used two-photon time-lapse imaging of *Tg(tagln:nls-egfp-2a-cfp-f)*^{y450} transgenic animals in which the *tagln* promoter drives expression of both nuclear-targeted EGFP and membrane-targeted farnesylated CFP (Fig. 2L) in order to track the nuclei of mural cells contributing to the dorsal aorta. We collected 1- to 2-day-long time-lapse sequences beginning at approximately 2.5 dpf. Although most dorsal aorta-juxtaposed EGFP-positive nuclei appeared to move little if at all during time lapse imaging, in a few particularly striking examples the cells could be observed migrating from the sclerotome on one side of the aorta to take up position on the other side of the aorta (Fig. 2M, Movie 1). Other aorta-associated EGFP-positive cells were lost to analysis for technical reasons (i.e. difficulty in following the nuclei because of low fluorescence, too many adjacent cells to distinguish nuclei, lack of movement, etc.). In no case however were any cells traced to tissues or sites of origin other than adjacent to the aorta in and/or near the sclerotome. Interestingly, despite lack of substantial movement of most aorta-associated nuclei in *Tg(tagln:nls-egfp-2a-cfp-f)*^{y450} transgenic animals, it was relatively easy to observe bulk movement of EGFP-positive cell membranes from the sclerotome to become more closely associated with the adjacent dorsal aorta in *Tg(tagln:egfp)* transgenic animals (Fig. S4D,E, Movie 2). Taken together, these data suggest that vSMC precursors are moving relatively small distances from the adjacent sclerotome to become associated with the dorsal aorta, with nuclei that may even remain relatively stationary. Once the initial population of vSMCs become associated with the dorsal aorta and intersegmental vessels, further increases in mural cell coverage of the trunk vasculature appear to occur, at least in part, via proliferation of the initial cell population (Fig. S5). The findings we describe above are entirely consistent with a study recently published by Ando et al. (2016).

Disrupting PDGF signaling interferes with mural cell recruitment

In order to examine the functional role of dorsal aorta-associated mural cells in the early embryo and larva, we inhibited their recruitment to the developing dorsal aorta by disrupting PDGF signaling (Lindblom et al., 2003; Lindahl et al., 1997; Hellstrom et al., 1999; Armulik et al., 2011a). We utilized a *Tg*(*UAS:pdgfrbDN-YFP)* transgenic zebrafish to inducibly express a PDGFRβ construct containing intact N-terminal PDGF ligand binding and transmembrane domains but with the intracellular signaling domain replaced by YFP. This C-terminally truncated PDGFRβ has previously been shown to act in a dominant-negative

Development (2017) 144, 115-127 doi:10.1242/dev.143131

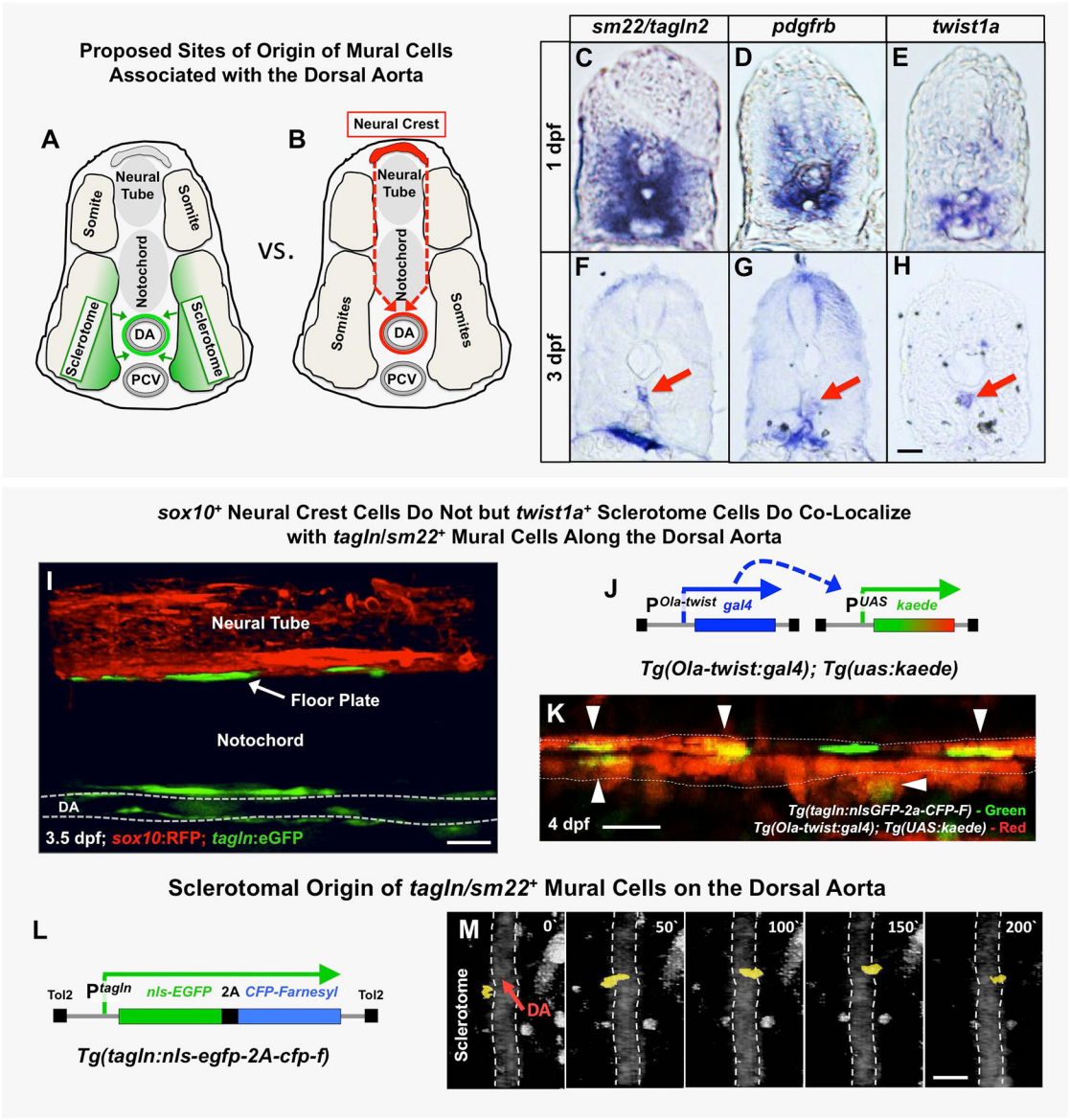

Fig. 2. The origins of trunk vSMCs. (A,B) Schematic diagrams illustrating two alternative models for the origin and migration of vSMCs recruited to the dorsal aorta, either from the sclerotome (A) or from the trunk neural crest (B). (C-H) Transverse sections of the trunk from 1 dpf (C-E) or 3 dpf (F-H) animals subjected to whole-mount *in situ* hybridization expression analysis, probed with *tagln2* (C,F), *pdgfrb* (D,G) or *twist1a* (E,H). All three markers are expressed more broadly in the sclerotome at 1 dpf (C-E), but by 3 dpf their expression becomes restricted to SMCs of the DA (red arrows) and gut (F,G) or DA alone (H). (I) Confocal lateral view image of the mid-trunk of a 3.5 dpf *Tg(tagln:gfp), Tg(sox10:rfp)* double transgenic animal. The lack of RFP expression along the dorsal aorta suggests *tagln*$^{+}$ vSMCs are not of neural crest origin. DA, dorsal aorta. (J) Schematic diagram of the *Tg(Ola-twist:gal4)* and *Tg(uas:kaede)* transgenes. In *Tg(Ola-twist:gal4)*, *Tg(uas:kaede)* double transgenic fish, the medaka (*Oryzias latipes) twist* promoter (Ola-twist) is used to drive expression of Gal4 from the *Ola-twist:gal4* transgene, which then activates expression of green to red photoconvertible kaede from the *uas:kaede* transgene. (K) Confocal lateral view image of the dorsal aorta in a 4 dpf *Tg(Ola-twist:gal4), Tg(uas:kaede), Tg(tagln:nlsGFP-2a-CFP-F)* triple-transgenic animal in which sclerotome-expressed kaede was photoconverted to red fluorescence at 4 dpf to mark *twist1*-positive cells. Numerous double-positive *tagln*$^{+}$ (green nucleus), *twist*$^{+}$ (red cytoplasm) cells are clearly evident on the dorsal aorta (arrowheads). A total of five fish were imaged in two rounds of photoconversion experiments with equivalent results. (L) Schematic diagram of the *Tg(tagln:nlsgfp-2a-cfp-f)* transgene, with the *tagln* promoter driving expression of nuclear-localized GFP and membrane-localized farnesyl CFP, joined by a 2A peptide linker. (M) Selected frames from a confocal time-lapse image series collected from a *Tg(tagln:nlsgfp-2a-cfp-f), Tg(kdrl:mCherryCAAX)* double-transgenic fish shows the movement of a *tagln*$^{+}$ nucleus (yellow) from the adjacent sclerotome to the dorsal aorta (demarcated by dashed lines). The image reconstructions shown are ventral views, with rostral to the top. Confocal images were acquired every 10 min and the displayed stills are shown at approximately 50 min intervals. In total, seven *tagln*$^{+}$ nuclei investing the DA were traced to the sclerotome in five separate time-lapse experiments. Scale bars: 50 µm.

fashion and to have effects on vSMC recruitment to anterior regions of the dorsal aorta when injected as a mosaic construct (Wiens et al., 2010; Fortuna et al., 2015).

We began by driving heat shock-inducible global expression of the dominant-negative PDGFRβ by crossing the *Tg(UAS:pdgfrbDN-YFP)* transgenic line to the *Tg(hsp70:gal4)* driver line (Scheer and Campos-Ortega, 1999) (Fig. 3A). By also including the *Tg(tagln:egfp)* transgenic background and using auto-fluorescence of circulating red blood cells to mark the vascular compartment we could easily assess mural cell recruitment to the dorsal aorta in these

Development (2017) 144, 115-127 doi:10.1242/dev.143131

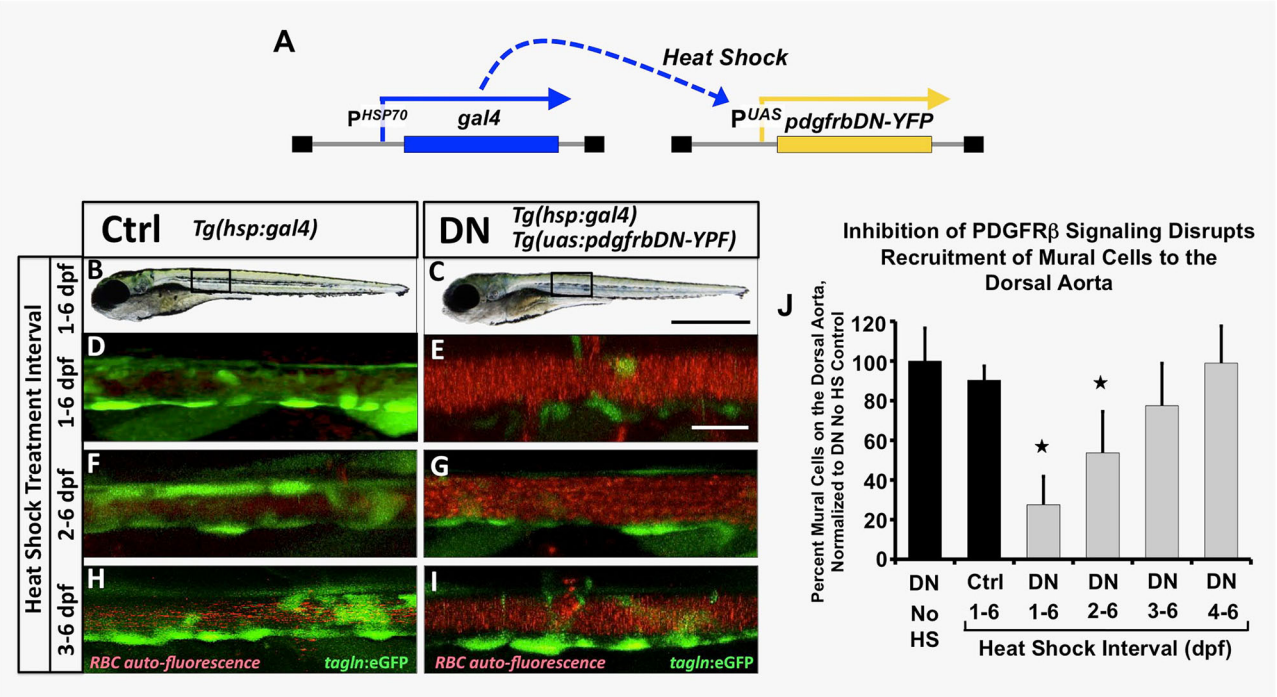

Fig. 3. Inhibition of *pdgfr* signaling leads to loss of mural cell coverage on the dorsal aorta. (A) Schematic diagram showing the *Tg(HSP70:gal4* and *UAS:pdgfrbDN-YFP)* double transgenes used for heat shock-inducible expression of *pdgfrbDN*. These fish were outcrossed to *Tg(tagln:egfp)* transgenic fish to generate triple heterozygotes, heat shocked daily for the indicated time frame and imaged for analysis of mural cell coverage at 6 dpf. (B-I) Representative confocal images of 6 dpf heat shocked *Tg(tagln:egfp), Tg(HSP70:gal4)* control (Ctrl, B,D,F,H) or *Tg(tagln:egfp), Tg(HSP70:gal4), Tg(UAS:pdgfrbDN-YFP)* dominant negative-expressing (DN, C,E,G,I) animals are shown. Fish were heat shocked daily from 1-6 dpf (B-E), 2-6 dpf (F-G) or 3-6 dpf (H-I) and then imaged at 6 dpf. The *tagln*/*sm22*$^{+}$ vSMCs associated with the dorsal aorta are shown in green; red blood cell autofluorescence showing the vascular compartment is in red. (J) Quantification of the number of vSMCs covering the dorsal aorta following the indicated heat shock interval. *Tg(tagln:egfp), Tg(HSP70:gal4), Tg(UAS:pdgfrbDN-YFP)* heat shock-inducible dominant negative PDGFRB (DN) or *Tg(tagln:egfp), Tg(HSP70:gal4)* control (Ctrl) fish were heat shocked as indicated, imaged at 6 dpf and the number of *tagln*/*sm22*$^{+}$ cells per 3-somite segment length of dorsal aorta counted. Values were normalized to the *tagln*/*sm22*$^{+}$ cell counts from non-heat shocked DN fish. Values are mean±s.e.m.; *P≤0.05 significance compared with non-heat shocked DN fish. Data are presented from a single experiment of n=5 fish; two experimental replicates for 2, 3, 4 day HS experiments and four experimental replicates from 1-6 day HS were carried out as validation showing consistent results. In more absolute values, we typically see approximately 20 vSMCs recruit to a 3-somite segment of dorsal aorta under control conditions, and ∼7-8 vSMCs recruit to a 3-somite length of dorsal aorta under DN activation conditions. Scale bars:1 mm (B,C) and 50 µm (D-I).

animals. Heat shock induction of *Tg(hsp70:gal4)/+, Tg(UAS:pdgfrbDN-YFP)/+* double transgenic embryos or control *Tg(hsp70:gal4)/+* siblings was initiated beginning at 1, 2, 3 or 4 dpf, with daily heat shock cycles continuing until vSMC coverage was assessed at 6 dpf by confocal imaging (Fig. 3B-J). Early heat shock-inducible global expression of the *pdgfrbDN* led to strongly reduced vSMC recruitment to the zebrafish dorsal aorta, with fewer defects noted if heat shock was initiated later, after vSMCs have started to migrate towards the dorsal aorta at 2 to 3 dpf (Fig. 3E,G,I,J). No gross morphological defects (Fig. 3B,C) or vascular patterning defects (Fig. S6) were noted in heat-shocked double-transgenic animals. Non-heat shocked *Tg(hsp70:gal4)/+, Tg(UAS:pdgfrbDN-YFP)/+* double transgenic animals (Fig. 3J, first column) or heat-shocked control *Tg(hsp70:gal4)/+* transgenic siblings (Fig. 3B,D,F, H, and J, second column) showed no defects in vSMC recruitment.

To further examine the requirement for PDGF signaling more specifically in vSMCs and minimize potential off-target or pleiotropic effects, we generated a new *Tg(tagln:EcRgal4)*^{v449} transgenic line in order to drive tebufenozide-inducible expression of *pdgfrbDN* in vSMCs when crossed to the *Tg(UAS:pdgfrbDN-YFP)* line (Fig. S7A). Tebufenozide was added to *Tg(tagln:EcRgal4)/+, Tg(UAS:pdgfrbDN-YFP)/+* double-transgenic animals in the *Tg(tagln:egfp)* background beginning at 0.5 dpf with daily replacement of the drug. vSMC association with the dorsal aorta was analyzed at 6 dpf, utilizing red blood cell auto-fluorescence to visualize the vascular compartment. Animals to which tebufenozide was added to induce expression of *pdgfrbDN* showed strongly reduced numbers of *tagln:egfp*-positive vSMCs associated with the dorsal aorta (Fig. S7C,E,G, and H, light gray column) compared with their non-tebufenozide treated sibling controls (Fig. S7B,D,F, and H, black column). Tebufenozide treatment of *Tg(tagln:EcRgal4)/+* single-transgenic siblings also has no effect on vSMC coverage (Fig. S7H, dark gray column). These data support a role for mural cell-autonomous PDGF signaling in the development and stabilization of the vascular wall.

Mural cell recruitment restricts aortic diameter and promotes assembly of vascular basement membranes

Previous studies have shown that the diameter of the dorsal aorta (DA) and posterior cardinal vein (PCV) decreases as development proceeds in the zebrafish (Bagatto and Burggren, 2006). During normal development, aortic diameter is inversely correlated with accumulation of mural cells over time (Fig. 4A-C), suggesting a possible relationship between the two phenotypes. To examine whether mural cell coverage plays a role in restricting aortic diameter, we examined aortas in heat shock control versus *Tg(hsp70:gal4)/+, Tg(UAS:pdgfrbDN-YFP)/+, Tg(kdrl:mCherry)* triple transgenic animals (Fig. 4D-F) and in tebufenozide-treated

Development (2017) 144, 115-127 doi:10.1242/dev.143131

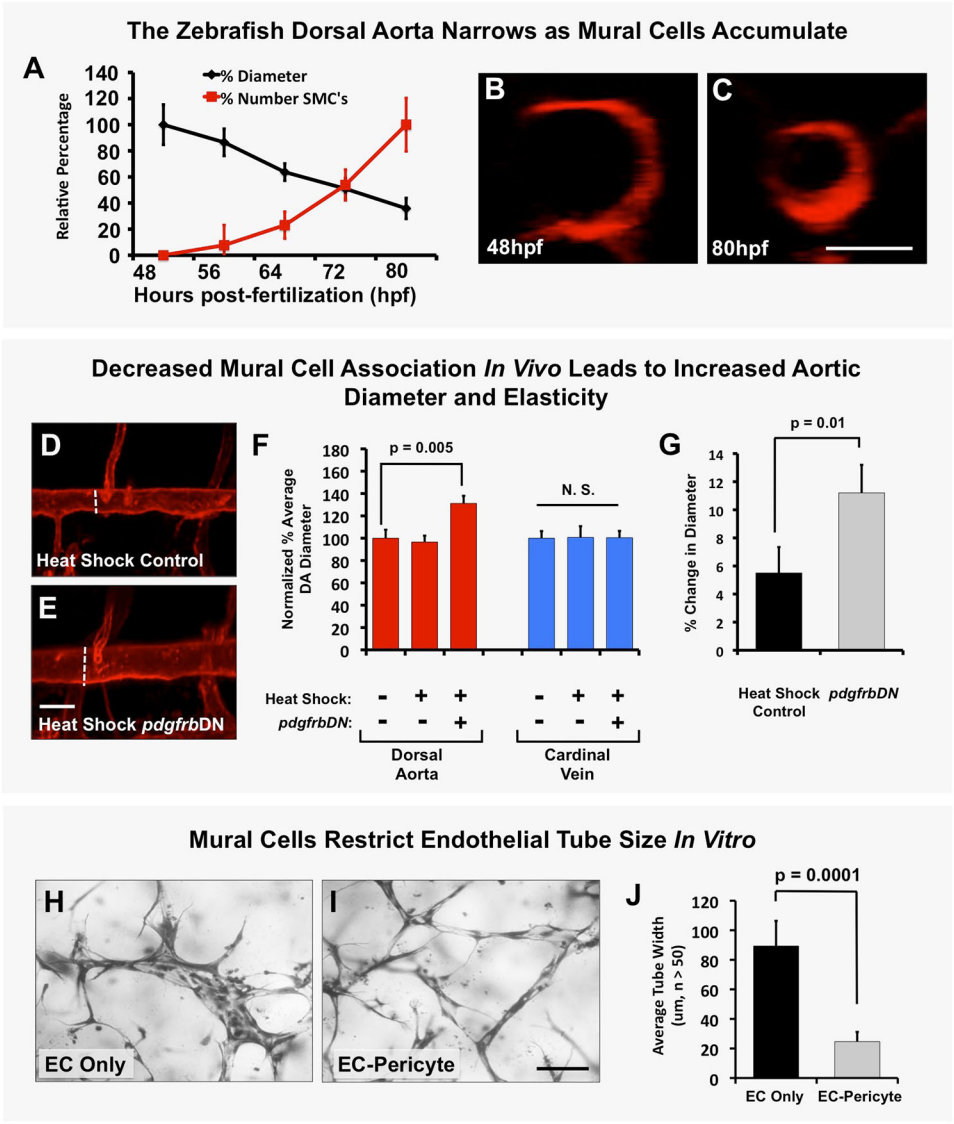

Fig. 4. Mural cells regulate aortic diameter and elasticity. (A) Accumulation of vSMCs on the dorsal aorta inversely correlates with reduced dorsal aorta diameter over time during zebrafish vascular development. Dorsal aorta diameter is normalized to starting 48 hpf value and vSMC number is normalized to final 80 hpf value. *n*=3 fish. (B,C) Representative 2 dpf (B) and 3.25 dpf (C) transverse reconstructions of confocal images of the dorsal aorta in *Tg(kdrl:mCherryCAAX)* transgenic zebrafish, shown at the same magnification. (D,E) Loss of mural cell coverage leads to expansion of the zebrafish dorsal aorta. Representative 5 dpf confocal images of the mid-trunk dorsal aorta in *Tg(kdrl:mCherryCAAX), Tg(tagln:egfp), Tg(HSP70:gal4)* control (D) or *Tg(kdrl:mCherryCAAX), Tg(tagln:egfp), Tg(HSP70:gal4), Tg(UAS:pdgfrbDN-YFP)* dominant negative *pdgfrbDN* transgene-expressing (E) embryos that were heat shocked for a full 1-5 day time course. (F) Quantification of dorsal aorta diameter, demonstrating marked expansion of the dorsal aorta in heat shock *pdgfrbDN* fish compared with non-heat shocked or heat shocked control siblings. No effects were noted on the diameter of the cardinal vein. A minimum of three fish were measured per sample, with ten separate dorsal aorta measurements per fish. Experiments were repeated three times showing consistent results; N.S., not significant. (G) Loss of vSMC coverage leads to increased elasticity of the dorsal aorta in the developing zebrafish embryo. Heat shock control (maintains vSMC coverage) versus heat shock *pdgfrbDN* (demonstrates marked loss of vSMC coverage) fish were imaged using SPIM. Images were acquired at 22 frames per second to capture the movement of the wall of the dorsal aorta ('elasticity') as it expands and retracts in accordance with the animal's heartbeat. Data are reported as a percentage diameter change [(maximal width of the aorta-minimal width of the aorta)/minimal width of the aorta×100]. Five fish were measured per sample, with three separate dorsal aorta measurements taken per fish. Mean±s.e.m. (H-J) Regulation of EC tube diameter by mural cells can be modeled in 3D collagen matrix assays *in vitro*. Representative images of EC-only culture (H) and EC-pericyte co-cultures (I) are shown. (J) Quantification of endothelial tube diameter in EC-only cultures and EC-pericyte co-cultures established in 3D collagen matrices, showing a marked reduction in EC tube diameter in the presence of mural cells (pericytes). *n*=5 images from separate collagen plugs, ten measurements per image. Scale bars: 50 µm. Values are mean±s.d.

versus untreated *Tg(tagln:EcRgal4)/+, Tg(UAS:pdgfrbDN-YFP)/+* double-transgenic animals (Fig. S7I). The diameter of the dorsal aorta was significantly larger in animals in which *pdgfrbDN* was induced by heat shock (Fig. 4D-F) or tebufenozide treatment (Fig. S7I), while the diameter of the posterior cardinal vein (which becomes invested by mural cells mostly after 6 dpf – see Fig. S1) was not significantly increased (Fig. 4F, Fig. S7I). This phenomenon was also readily modeled *in vitro*, where ECs seeded alone in collagen type I gels formed tubes that continued to increase in diameter over time, while ECs seeded together with pericytes formed tubes that recruited pericytes and maintained a restricted diameter (Fig. 4H-J).

Development (2017) 144, 115-127 doi:10.1242/dev.143131

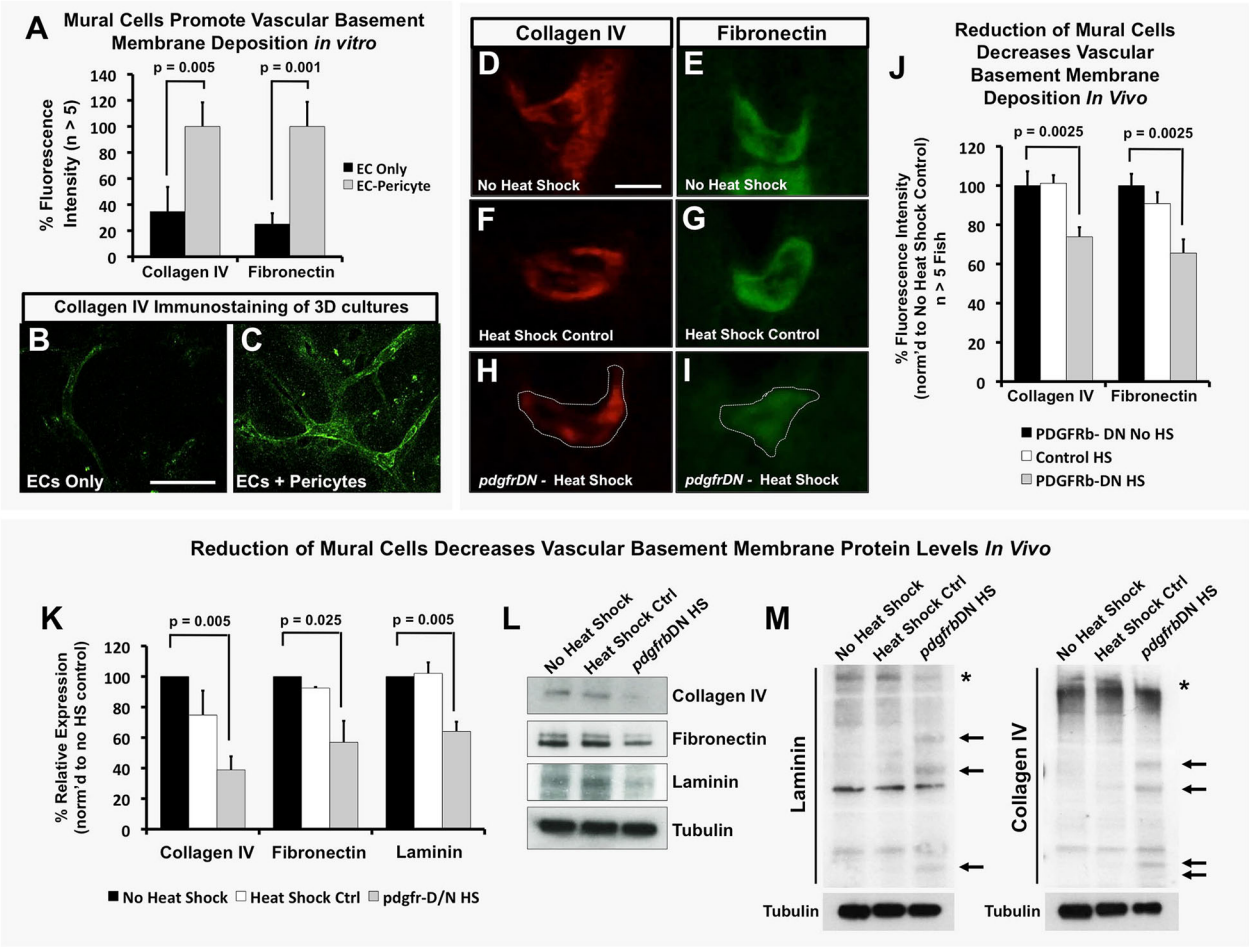

Fig. 5. EC-mural cell interactions promote deposition and maintenance of the vascular basement membrane. (A-C) Mural cells promote vascular basement membrane deposition *in vitro*. (A) Quantification of basement membrane components collagen IV and fibronectin in 3D collagen matrix assays with ECs alone (black) or EC-pericyte co-cultures (gray) using detergent-free immunostaining protocols to assess only the extracellular deposition of these proteins. Representative images of collagen IV staining in EC only (B) and EC-pericyte co-cultures (C); *n*>5 individual immunostained collagen plugs. (D-J) vSMCs promote vascular basement membrane deposition and stability *in vivo*. (D-I) Representative images of collagen IV (D,F,H) or fibronectin (E,G,I) immunostaining of the dorsal aorta in transverse paraffin sections of 5 dpf no heat shock double transgenic *Tg(HSP70:gal4; UAS:pdgfrbDN-YFP)* animals (D,E), 1-5 dpf heat-shocked control *Tg(HSP70:gal4)* animals (F,G) or 1-5 dpf heat-shocked *pdgfrbDN*-expressing double transgenic *Tg(HSP70:gal4; UAS:pdgfrbDN-YFP)* animals (H,I). (J) Quantification of 5 dpf dorsal aorta collagen IV or fibronectin immunostaining intensity using the relative basement membrane staining intensity of sections such as those shown in D-I. All data are shown as a percentage of the no heat shock control condition. *n*=10 fish total, combined data from three individual experiments. (K) Quantification of basement membrane protein levels by western blot analysis (*n*=3 blots, from three individual experiments) of each of the conditions shown in D-J. Data are represented as a percentage of the no heat shock control condition. (L) Representative western blot images are shown versus a tubulin loading control. (M) The ability of mural cells to regulate maintenance of full-length basement membrane components was analyzed by collecting protein lysates under non-reducing conditions. No heat shock control, heat shock control (not carrying the *pdgfrbDN* cassette) and *pdgfrbDN*, heat shock treatment lysates were collected for analysis of protein fragmentation levels of collagen IV and laminin proteins. Representative western blots are shown, with increased fragmentation (highlighted by arrows) of the proteins noted only in the *pdgfrbDN* heat shock condition, where mural cell coverage has been disrupted. Location of the full-length proteins is marked with an asterisk. Representative western blots from lysates of ten pooled zebrafish embryos and two individual experiments. Scale bars: 50 µm. Values are mean±s.e.m.

Heat shocked *Tg(hsp70:gal4)/+, Tg(UAS:pdgfrbDN-YFP)/+, Tg(fli:egfp)* animals also showed significantly greater vessel wall elasticity compared with their heat shocked control siblings (Fig. 4G; Movie 3). Using single plane illumination microscopy (SPIM) to measure the magnitude of the rapid changes in vessel diameter occurring in conjunction with the beating of the heart, we showed that heat shocked *Tg(hsp70:gal4)/+, Tg(UAS:pdgfrbDN-YFP)/+, Tg(fli:egfp)* had a nearly 12% change in dorsal aorta diameter with each heartbeat compared with less than 6% in heat shocked *Tg(hsp70:gal4)/+, Tg(fli:egfp)* sibling control animals (Fig. 4G; Movie 3).

Since previous evidence suggests that basement membrane formation is required to help restrict vessel expansion (Davis and Senger, 2005; Hynes, 2007; Jain, 2003; Stratman et al., 2009, 2010; Stratman and Davis, 2012) and that production/stabilization of basement membrane proteins is in part mediated by EC-mural cell interactions, we examined whether EC-mural cell interaction could be modulating the assembly of the vascular basement membrane of the developing zebrafish dorsal aorta. *In vitro* cultures of ECs alone show a lack of extracellular deposition of basement membrane matrix structural components, such as collagen IV and fibronectin, compared with cultures seeded with both ECs and pericytes (Fig. 5A-C), suggesting that the presence of both cell types is required to maintain a vascular basement membrane. We used our vSMC-deficient zebrafish models to examine whether this is

Development (2017) 144, 115-127 doi:10.1242/dev.143131

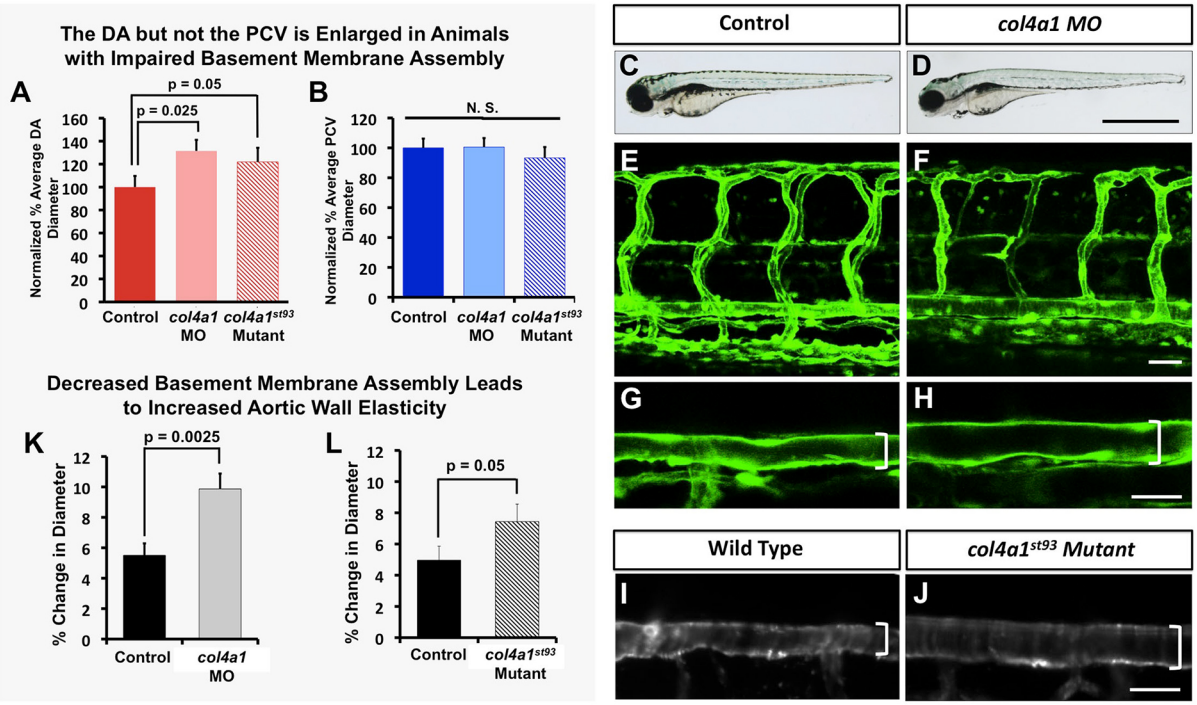

Fig. 6. The vascular basement membrane functionally regulates aortic diameter and stability. Impaired basement membrane assembly leads to increased aortic diameter and elasticity. (A,B) Quantification of dorsal aorta (A) and posterior cardinal vein (B) diameter in 4 dpf *col4a1* morpholino-injected or *col4a1*$^{st93/st93}$ mutant animals compared with control wild-type animals. A minimum of four fish were measured per sample, with ten separate dorsal aorta measurements per fish. N.S., not significant. (C-J) Representative transmitted light (C,D) and confocal (E-J) images of 4 dpf control (C,E,G,I), *col4a1* morpholino-injected (D,F,H), or *col4a1*^{st93} mutant (J) animals, showing lateral views of entire animal (C,D) lateral views of the trunk vasculature (E,F) and higher-magnification lateral images of the dorsal aorta (G-J). Brackets indicate diameter of dorsal aorta. (K,L) Quantification of dorsal aorta elasticity in 4 dpf *col4a1* morpholino-injected (K) or *col4a1*^{st93} mutant (L) animals compared with control wild-type animals, using SPIM. Data are reported as percentage diameter change. A minimum of four fish were measured per sample, with three separate dorsal aorta measurements made per fish. Scale bars: 50 µm. Values are mean±s.e.m.

similarly the case *in vivo*. In the 5 dpf zebrafish trunk, deposition of structural components of the vascular basement membrane, including laminin, fibronectin and collagen IV, is concentrated around the developing dorsal aorta, as assessed by immunofluorescence staining of transverse trunk tissue sections with specific antibodies (Fig. S8A and Fig. S9). Heat shock treatment of *Tg(hsp70:gal4)/+, Tg(UAS:pdgfrbDN-YFP)/+* double-transgenic animals significantly reduced the amount of antibody-positive immunostaining for collagen IV and fibronectin present around the 5 dpf dorsal aorta (Fig. 5D-J). Protein lysates from these same animals showed significant decreases in the full-length forms of collagen IV, laminin and fibronectin (Fig. 5K,L). By collecting protein lysates under non-reducing conditions, we could also show an increase in fragmented forms of collagen IV and laminin proteins in heat-shocked *Tg(hsp70:gal4)/+, Tg(UAS:pdgfrbDN-YFP)/+* double-transgenic animals compared with heat shocked control or no heat shock double transgenic animals (Fig. 5M).

To further examine whether the basement membrane restricts aortic diameter and elasticity, we disrupted a key structural component of the basement membrane, collagen IV (*col4a1* in zebrafish). Animals that were either injected with *col4a1* translation-blocking morpholino or homozygous for the *col4a1*$^{st93/st93}$ mutation displayed increased aortic diameter (Fig. 6A,C-J) similar to that seen in vSMC-deficient animals (Fig. 4D-F, Fig. S7I). Overall vascular patterning (Fig. 6E,F) and blood flow (Movie 4) were not significantly altered in any of the animals analyzed for these studies. Using SPIM to measure changes in vessel wall elasticity, we showed that there was a ~5-6% change in dorsal aorta diameter with each beat of the heart in control animals, whereas in *col4a1* morpholino-treated animals or *col4a1*$^{st93/st93}$ mutants there was an approximate 10% and 7-8% change in diameter with each heartbeat, respectively (Fig. 6K,L Movie 4).

DISCUSSION

We have examined the ontogeny and functional role of vSMCs surrounding the dorsal aorta during early stages of zebrafish development. Using a combination of molecular markers, transgenic lines and live imaging, we show that a subpopulation of cells from the sclerotome appears to delaminate and differentiate into vSMCs recruited to the dorsal aorta. These cells serve an important functional purpose: to restrict aortic diameter by facilitating assembly and maintenance of the vascular basement membrane. Reducing vSMC recruitment by disrupting PDGF signaling results in defects in basement membrane formation around the dorsal aorta, failure to restrict dorsal aorta diameter and increased dorsal aorta elasticity, as measured using SPIM. Dorsal aorta diameter and elasticity are also increased by directly disrupting the vascular basement membrane component *col4a1*, supporting a crucial role for vSMC-promoted basement membrane assembly in regulating the growth and size of vessels during development (Fig. 7).

Ontogeny of vSMCs associated with the zebrafish dorsal aorta

Previous reports from the zebrafish and studies from chick/quail and murine models have supported a model whereby mesodermal-

Development (2017) 144, 115-127 doi:10.1242/dev.143131

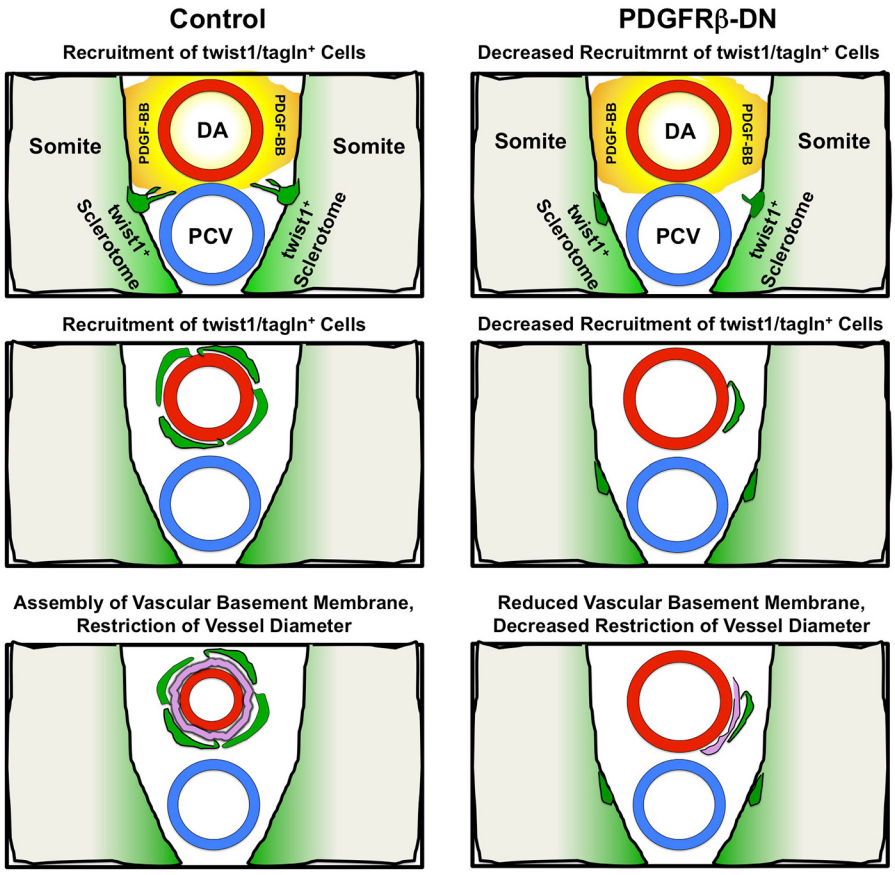

Fig. 7. Mural cells regulate vascular outgrowth and stability through deposition of the basement membrane. Schematic representation of the role mural cells play in stabilization of blood vessels. Under control conditions, mural cells (green) delaminate from the sclerotome to associate with the dorsal aorta (red). These cells interact with the endothelium to promote basement membrane protein deposition and maintenance (pink). Under conditions in which mural cell recruitment is inhibited (i.e. *pdgfrbDN*) vascular stabilization is markedly disrupted and reduced basement membrane deposition is noted.

derived cells contribute to the host population of cells that become vSMCs along the dorsal aorta (Bergers and Song, 2005; Majesky, 2007; Pouget et al., 2008; Wiegreffe et al., 2007; Wasteson et al., 2008; Armulik et al., 2011a). Through use of transgenic reporters and nuclear tracking studies, we demonstrate that the majority of vSMCs that end up resident on the dorsal aorta in the zebrafish trunk are *twist1*$^{+}$ cells derived from the sclerotome, not *sox10*$^{+}$ neural crest-derived cells. Our findings are entirely consistent with previous mammalian reports and with a well-documented recent report in the zebrafish from Ando et al. (2016) that identified the paraxial and lateral plate mesoderm as the source of mural cells in the trunk. Together with those of Ando et al. (2016), our data suggest that most early dorsal aorta vSMC progenitors emerge from the immediately adjacent *twist1*$^{+}$ sclerotomal compartment of the somites, and in most cases appear to move little distance before investing the dorsal aorta. As with any experiments designed to mark and track vSMCs to determine their origins, it is difficult to completely exclude any contribution from other anatomical sites of origin, particularly as many of the transgenic markers used to mark vSMCs tend to start being expressed just as these cells are undergoing differentiation, complicating execution and interpretation of these experiments. Although our data and those of Ando et al. (2016) strongly implicate sclerotomal progenitors as the major source of vSMCs investing the dorsal aorta, and demonstrate clearly that neural crest-derived cells do not contribute to aortic vSMCs, additional rigorous lineage-tracing experiments would be needed to fully rule out alternative sources for vSMCs in the trunk. While not the main focus of the present study, further more comprehensive examination of the ontogeny of vSMCs and migratory patterns and pathways used by early trunk vSMC progenitors would be useful.

A large body of work has exhaustively documented the crucial role that PDGF-BB/PDGFRβ signaling plays in mural cell recruitment to blood vessels in a variety of models. Consistent with these studies (Hellstrom et al., 1999; Lindahl et al., 1997; Lindblom et al., 2003; Bergers and Song, 2005; Stratman et al., 2010; Hirschi et al., 1999; Lehti et al., 2005; Fortuna et al., 2015; Armulik et al., 2011a), our work also suggests that PDGF signaling is required for proper vSMC recruitment to the dorsal aorta. Global (Fig. 3) or vSMC-autonomous (Fig. S7) inducible expression of a dominant-negative *pdgfrbDN* transgene results in defects in vSMC recruitment to the dorsal aorta without evidence of any significant effects on gross anatomy or vessel growth. The inhibition of vSMC recruitment is not complete in our *pdgrfrbDN* experiments. This raises the possibility that other mechanisms besides PDGF signaling may also be used to help vSMC 'home' to vessels (Lee et al., 2007; Higashiyama et al., 1993; Iivanainen et al., 2003; Krymskaya et al., 1997; Wang et al., 2014, 2012; Kofler et al., 2015; Fortuna et al., 2015; Kennard et al., 2008; Hirschi et al., 2003; Aplin et al., 2010; Stratman et al., 2010; Zaucker et al., 2013). However, it is also possible that we are simply not able to sufficiently eliminate vSMC PDGF signaling using this method and that residual vSMC recruitment reflects this 'bleed through'. Further studies will be needed to determine which of these possibilities is true. Although previous reports utilizing this *pdgfrbDN* line suggest alterations in ISV outgrowth (Wiens et al., 2010), we did not note these phenotypes in our heat shock experiments (we initiated heat shock no earlier than 24 hpf, Fig. S6). Additionally, we took the extra step of generating a new *Tg(tagln:EcRgal4)*^{v449} tebufenozide-inducible vSMC driver line to provide stronger evidence that the results we obtained reflected vSMC-autonomous effects. Previous

Development (2017) 144, 115-127 doi:10.1242/dev.143131

reports have described *pdgfrb* zebrafish mutants lacking marked effects on vSMC recruitment (Kok et al., 2015; Ando et al., 2016). However, other studies utilizing mosaic injection of the *pdgfrbDN* construct and the PDGFRβ inhibitor, inhibitor V, in zebrafish (in addition to the data shown in our study) have documented significant effects of activation of this construct on vSMC recruitment to the dorsal aorta (Fortuna et al., 2015; Fig. 3, Fig. S7). The discrepancy between vSMC phenotypes in zebrafish *pdgfrbDN* expression studies and mouse PDGF-BB and PDGFRβ knockout/knock-in studies as compared with the lack of phenotype in zebrafish *pdgfrb* mutants might reflect genetic compensation in zebrafish *pdgfrb* mutants (Rossi et al., 2015). The *pdgfrb* and *pdgfra* receptors are known to dimerize, and it is likely that the *pdgfrbDN* dominant-negative construct would prevent compensation of one receptor by the other, something that is much less likely to occur in the *pdgfrb* zebrafish mutants. Although further work will be needed to fully unravel the roles of specific PDGF receptors and ligands in vSMC development in the fish, it is clear from our data and other previous reports that the *pdgfrbDN* construct provides a useful tool to disrupt vSMC recruitment to the dorsal aorta as a way to functionally study the consequences of loss of this cell population on vascular stabilization.

The crucial function of the vascular basement membrane during development

Assembly of the vascular basement membrane is contingent on two fundamental processes: (1) synthesis and deposition of all of the individual components, and (2) maintenance of these components (Yurchenco, 2011; Francis et al., 2002; George et al., 1993; Jain, 2003; Davis and Senger, 2005; Hynes, 2007). A variety of reports have suggested that cooperation between ECs and vSMCs/pericytes is needed to properly synthesize and maintain all components of the vascular basement membrane niche (Stratman et al., 2009, 2010; Abraham et al., 2008; Smola et al., 1998; Stratman and Davis, 2012). A number of *in vitro* studies have shown that while ECs can synthesize the majority of basement membrane proteins in an autonomous fashion, vSMCs and pericytes provide a number of proteolytic inhibitors, such as TIMPs, that can prevent the basement membrane from undergoing degradation by EC-generated MMPs (Saunders et al., 2006; Stratman et al., 2009; Mascall et al., 2012; Castoldi et al., 2003; Stratman and Davis, 2012). Pericytes have also been reported to generate a high abundance of proteins, such as nidogen-1, and proteoglycans that serve to crosslink and stabilize many of the main structural components of basement membranes, such as laminin, collagen IV and fibronectin (Yurchenco, 2011; Perkins et al., 1979; Jain, 2003; Breitkreutz et al., 2004; Hynes, 2007; Stratman et al., 2009). Although additional studies are needed to further understand the molecular mechanisms involved, including the use of cell type-specific gene suppression strategies *in vivo*, the data suggest strongly that ECs and mural cells are required in tandem to build and maintain the vascular basement membrane.

Our findings using experimental manipulation of intact animals and live imaging in the zebrafish now provides evidence that EC-mural cell interactions are indeed essential for maintenance of the vascular basement membrane. We show that loss of vSMC coverage leads to marked decreases in stabilization of full-length collagen IV and fibronectin and decreased accumulation of these proteins around the dorsal aorta (Fig. 5). Loss of proper basement membrane formation translates to changes in blood vessel morphology and dynamics, including increased diameter of the dorsal aorta and increased elasticity of the vascular wall (Figs 4 and 6, Fig. S7). These changes might also be expected to lead to alterations in blood pressure, shear stress and even flow directionality *in vivo*, analogous to phenotypes that present in many disease states such as stroke and atherosclerosis, suggesting that disruption of these fundamental cell-cell interactions could be a factor in the vascular dysfunction in these pathologies.

Concluding remarks

Our study and other recent work (Ando et al., 2016; Fortuna et al., 2015; Santoro et al., 2009; Wang et al., 2014; Whitesell et al., 2014; Seiler et al., 2010; Miano et al., 2006; Vanhollebeke et al., 2015; Zaucker et al., 2013) demonstrate the utility of the zebrafish model for studying the recruitment and function of mural cells during vascular development. In addition to the transgenic lines and constructs described and validated in this report, a number of other recently generated tools have made it relatively easy to visualize and study this crucial cell population within an intact organism (Seiler et al., 2010; Whitesell et al., 2014; Santoro et al., 2009; Miano et al., 2006; Vanhollebeke et al., 2015). Furthermore, a number of functional studies have begun to assess the vital signaling pathways and functionality of mural cells during vascular development in the fish model. Ando et al. (2016) have generated a number of highly useful reporter constructs in addition to their work on studying mural cell ontogeny in the fish. Wang et al. (2014) carried out innovative work studying the combined roles of Notch signaling, mural cells and vascular integrity in the brain. The new tools developed for all of these studies will prove highly useful for future functional work focused on understanding vSMC development, recruitment and contribution to vascular stabilization.

MATERIALS AND METHODS

Zebrafish

Zebrafish (*Danio rerio*) embryos were raised and maintained as described (Westerfield, 1995; Kimmel et al., 1995). New transgenic lines generated include: Tg(*tagln:nls-egfp-2a-CFP-F*)^{y450} and Tg(*tagln:EcRgal4*)^{y449}. For details of established transgenic lines, see supplementary Materials and methods. Zebrafish husbandry and research protocols were reviewed and approved by the NICHD Animal Care and Use Committee at the National Institutes of Health. All animal studies were carried out according to NIH-approved protocols, in compliance with the Guide for the Care and use of Laboratory Animals.

Reagents

Antibodies for immunostaining and western blot analysis include: collagen IV (AbCAM, ab6586); fibronectin (AbCAM, ab6328); laminin (AbCAM, 11575); tubulin (Sigma, T6199); GFP (AbCAM, ab6556). Morpholino antisense oligonucleotides (Genetools) utilized include: 4 ng/µl *col4a1* translation blocking MO: ACACATGGAAGCCGCATC TTCACAC.

Generation of *col4a1*^{st93} allele

Transcription activator-like effector nucleases (TALENs; Sanjana et al., 2012) were employed to generate the *st93* allele. Sequencing identified *st93* as a 2 bp deletion in the ORF of *col4a1*, resulting in a frameshift from the wild-type sequence of 5′-CCT GGT CTA GAA GGA-3′ to 5′-CCT GGT CT–A AGG AGC-3′. This frameshift is predicted to change the protein sequence after the leucine residue at position 66 from PGLEGA to PGLRST and introduce a premature STOP codon at position 86 in the mutant allele. Details on generation of the allele can be found in supplementary Materials and methods.

TEM and immuno-EM

Zebrafish embryos (heads and tails removed) were fixed with 4% paraformaldehyde (PFA) with 0.5% glutaraldehyde in PBS. After fixation, the embryos were rinsed with PBS, dehydrated in ethanol and infiltrated in LR White resin, medium grade (Electron Microscopy Sciences,

Development (2017) 144, 115-127 doi:10.1242/dev.143131

Hatfield, PA) and finally embedded in 100% LR White resin. Polymerization of the resin was achieved using a Pelco UVC2 Cryo Chamber overnight at 4°C (Ted Pella, Redding, CA) as described in supplementary Materials and methods.

Time-lapse imaging and microscopy

Time-lapse images were collected utilizing either a Leica SP5 II or Olympus FV1000 confocal microscope starting at 56 hpf for *tagln* lines and 30 hpf for *Ola-twist* lines. Embryos were immobilized in buffered MS-222 and embedded in 0.8% low melting point agarose, with their heads and tail freed to facilitate continued growth. Images were acquired every 10 min for the desired time course. General microscopy for signal time points utilized the same confocal microscopes.

Heat shock and EcRgal4-driven *pdgfrbDN* activation

A daily 12 h heat shock program was developed to elicit maximal activation of the *pdgfrbDN* construct with minimal side effects on the growth and development of the zebrafish embryos. Further information on heat shock treatments can be found in supplementary Materials and methods. For EcRgal4-driven *pdgfrbDN* activation, tebufenozide resuspended in ethanol was added to the fish water at 100 µM. Water and drug were changed daily. Quantification of vSMC cell number was done by acquiring images of the zebrafish trunk starting at the 3-4 ISV and quantifying a 3-somite segment of dorsal aorta. Dorsal aorta width measurements were made using ImageJ by taking 10 individual measurements per image of the distance between the two walls of the aorta over a three somite segment length. Data are reported as a percentage of the control±s.e.m.

Endothelial cell culture and assays

HUVECs (Lonza) were cultured in bovine hypothalamus extract, 0.01% heparin and 20% FBS in M199 base medium (Gibco) on 1 mg/ml gelatin-coated tissue culture flasks. HUVECs were used from passages 3-6. Human pericytes (ScienCell) were cultured in 10% FBS in Advanced DMEM base medium (Gibco) on 1 mg/ml gelatin-coated tissue culture flasks. Pericytes were used from passages 3-10. Additional cell culture information can be found in the supplementary Materials and methods.

Immunostaining and western blot analysis

Zebrafish and 3D collagen assays utilized for immunostaining analysis were fixed in 4% or 2% PFA respectively at 4°C overnight. Zebrafish embryos were dehydrated in ethanol and embedded in paraffin for sectioning. Zebrafish samples for western blot analysis were de-yolked and directly lysed in 2× Laemmli sample buffer containing 5% b-ME and a PhosSTOP tablet (Roche), 10 µl per embryo unless otherwise indicated. Samples collected under native, non-reducing conditions did not contain β-ME. For further details, see supplementary Materials and methods.

qPCR and RNA extraction

Zebrafish embryos were collected at the indicated time points in Trizol and RNA purified using a double chloroform extraction protocol. cDNA was generated using a Bio-Rad I-Script cDNA synthesis kit from 500 ng RNA. SyberGreen qPCR protocols were utilized to generate relative expression data. Primer sets are available in the in the supplementary Materials and methods.

Dorsal aorta elasticity measurement methods

High-speed imaging of dorsal aorta movements were obtained using a lab-built light sheet microscope constructed using the Open-SPIM (Pitrone et al., 2013) wiki (www.openspim.org) with a VersaLase laser (Vortran Laser Technology) (488 nm/150 mW, 20% power), a Hamamatsu Orca R2 digital CCD camera, and a Picard Industries USB 4D Stage controlled by Fiji Micro-Manager open source software (Edelstein et al., 2010). Full details are available in in the supplementary Materials and methods.

Statistics

Statistical analysis of data was done using Microsoft Excel. Statistical significance was set at a minimum of $P \leq 0.05$ and is indicated in individual figures. Student's *t*-tests were used when analyzing two groups within a single experiment.

Acknowledgements

The authors would like to thank members of the Weinstein laboratory for their critical comments on this manuscript.

Competing interests

The authors declare no competing or financial interests.

Author contributions

A.N.S., S.A.P., O.M.F., D.C., M.G.B., H.S. and L.E.D. performed experiments; A.N.S., S.A.P., O.M.F., D.C., L.E.D., W.S.T. and B.M.W. analyzed results and made the figures; A.N.S., S.A.P., O.M.F., D.C. and B.M.W. designed the research and wrote the paper.

Funding

This work was supported by the intramural program of the Eunice Kennedy Shriver National Institute of Child Health and Human Development (ZIA-HD001011 and ZIA-HD008915 to B.M.W.), the National Institutes of Health (R01NS050223 to W.S.T.), an Agency for Science, Technology and Research (A*STAR) fellowship (to H.S.) and a National Heart, Lung, and Blood Institute/NIH K99 Pathway to Independence Award (to A.N.S.). Deposited in PMC for release after 12 months.

Supplementary information

Supplementary information available online at
http://dev.biologists.org/content/144/1/115.supplemental

References

Abraham, S., Kogata, N., Fassler, R. and Adams, R. H. (2008). Integrin beta1 subunit controls mural cell adhesion, spreading, and blood vessel wall stability. *Circ. Res.* **102**, 562-570.

Ando, K., Fukuhara, S., Izumi, N., Nakajima, H., Fukui, H., Kelsh, R. N. and Mochizuki, N. (2016). Clarification of mural cell coverage of vascular endothelial cells by live imaging of zebrafish. *Development* **143**, 1328-1339.

Aplin, A. C., Fogel, E. and Nicosia, R. F. (2010). MCP-1 promotes mural cell recruitment during angiogenesis in the aortic ring model. *Angiogenesis* **13**, 219-226.

Armulik, A., Genové, G., Mäe, M., Nisancioglu, M. H., Wallgard, E., Niaudet, C., He, L., Norlin, J., Lindblom, P., Strittmatter, K. et al. (2010). Pericytes regulate the blood-brain barrier. *Nature* **468**, 557-561.

Armulik, A., Genove, G. and Betsholtz, C. (2011a). Pericytes: developmental, physiological, and pathological perspectives, problems, and promises. *Dev. Cell* **21**, 193-215.

Armulik, A., Mäe, M. and Betsholtz, C. (2011b). Pericytes and the blood-brain barrier: recent advances and implications for the delivery of CNS therapy. *Ther. Deliv.* **2**, 419-422.

Bagatto, B. and Burggren, W. (2006). A three-dimensional functional assessment of heart and vessel development in the larva of the zebrafish (Danio rerio). *Physiol. Biochem. Zool.* **79**, 194-201.

Benjamin, L. E., Hemo, I. and Keshet, E. (1998). A plasticity window for blood vessel remodelling is defined by pericyte coverage of the preformed endothelial network and is regulated by PDGF-B and VEGF. *Development* **125**, 1591-1598.

Bergers, G. and Song, S. (2005). The role of pericytes in blood-vessel formation and maintenance. *Neuro Oncol.* **7**, 452-464.

Breitkreutz, D., Mirancea, N., Schmidt, C., Beck, R., Werner, U., Stark, H.-J., Gerl, M. and Fusenig, N. E. (2004). Inhibition of basement membrane formation by a nidogen-binding laminin gamma1-chain fragment in human skin-organotypic cocultures. *J. Cell Sci.* **117**, 2611-2622.

Castoldi, G., di Gioia, C. R. T., Pieruzzi, F., D'Orlando, C., Van, De Greef, W. M. M., Busca, G., Sperti, G. and Stella, A. (2003). ANG II increases TIMP-1 expression in rat aortic smooth muscle cells in vivo. *Am. J. Physiol. Heart Circ. Physiol.* **284**, H635-H643.

Chen, Z.-L., Yao, Y., Norris, E. H., Kruyer, A., Jno-Charles, O., Akhmerov, A. and Strickland, S. (2013). Ablation of astrocytic laminin impairs vascular smooth muscle cell function and leads to hemorrhagic stroke. *J. Cell Biol.* **202**, 381-395.

Daneman, R., Zhou, L., Kebede, A. A. and Barres, B. A. (2010). Pericytes are required for blood-brain barrier integrity during embryogenesis. *Nature* **468**, 562-566.

Davis, G. E. and Senger, D. R. (2005). Endothelial extracellular matrix: biosynthesis, remodeling, and functions during vascular morphogenesis and neovessel stabilization. *Circ. Res.* **97**, 1093-1107.

Edelstein, A., Amodaj, N., Hoover, K., Vale, R. and Stuurman, N. (2010). Computer control of microscopes using microManager. *Curr. Protoc. Mol. Biol.* **92**, 14.20.1-14.20.17.

Fortuna, V., Pardanaud, L., Brunet, I., Ola, R., Ristori, E., Santoro, M. M., Nicoli, S. and Eichmann, A. (2015). Vascular mural cells promote noradrenergic differentiation of embryonic sympathetic neurons. *Cell Rep.* **11**, 1786-1796.
Francis, S. E., Goh, K. L., Hodivala-Dilke, K., Bader, B. L., Stark, M., Davidson, D. and Hynes, R. O. (2002). Central roles of alpha5beta1 integrin and fibronectin in vascular development in mouse embryos and embryoid bodies. *Arterioscler. Thromb. Vasc. Biol.* **22**, 927-933.
Fujita, M., Cha, Y. R., Pham, V. N., Sakurai, A., Roman, B. L., Gutkind, J. S. and Weinstein, B. M. (2011). Assembly and patterning of the vascular network of the vertebrate hindbrain. *Development* **138**, 1705-1715.
George, E. L., Georges-Labouesse, E. N., Patel-King, R. S., Rayburn, H. and Hynes, R. O. (1993). Defects in mesoderm, neural tube and vascular development in mouse embryos lacking fibronectin. *Development* **119**, 1079-1091.
Germanguz, I., Lev, D., Waisman, T., Kim, C.-H. and Gitelman, I. (2007). Four twist genes in zebrafish, four expression patterns. *Dev. Dyn.* **236**, 2615-2626.
Hellstrom, M., Kalen, M., Lindahl, P., Abramsson, A. and Betsholtz, C. (1999). Role of PDGF-B and PDGFR-beta in recruitment of vascular smooth muscle cells and pericytes during embryonic blood vessel formation in the mouse. *Development* **126**, 3047-3055.
Higashiyama, S., Abraham, J. A. and Klagsbrun, M. (1993). Heparin-binding EGF-like growth factor stimulation of smooth muscle cell migration: dependence on interactions with cell surface heparan sulfate. *J. Cell Biol.* **122**, 933-940.
Hirschi, K. K., Rohovsky, S. A., Beck, L. H., Smith, S. R. and D'Amore, P. A. (1999). Endothelial cells modulate the proliferation of mural cell precursors via platelet-derived growth factor-BB and heterotypic cell contact. *Circ. Res.* **84**, 298-305.
Hirschi, K. K., Burt, J. M., Hirschi, K. D. and Dai, C. (2003). Gap junction communication mediates transforming growth factor-beta activation and endothelial-induced mural cell differentiation. *Circ. Res.* **93**, 429-437.
Hynes, R. O. (2007). Cell-matrix adhesion in vascular development. *J. Thromb. Haemost.* **5** Suppl. 1, 32-40.
Iivanainen, E., Nelimarkka, L., Elenius, V., Heikkinen, S.-M., Junttila, T. T., Sihombing, L., Sundvall, M., Määttä, J. A., Laine, V. J., Ylä-Herttuala, S. et al. (2003). Angiopoietin-regulated recruitment of vascular smooth muscle cells by endothelial-derived heparin binding EGF-like growth factor. *FASEB J.* **17**, 1609-1621.
Isogai, S., Lawson, N. D., Torrealday, S., Horiguchi, M. and Weinstein, B. M. (2003). Angiogenic network formation in the developing vertebrate trunk. *Development* **130**, 5281-5290.
Jain, R. K. (2003). Molecular regulation of vessel maturation. *Nat. Med.* **9**, 685-693.
Kennard, S., Liu, H. and Lilly, B. (2008). Transforming growth factor-beta (TGF- 1) down-regulates Notch3 in fibroblasts to promote smooth muscle gene expression. *J. Biol. Chem.* **283**, 1324-1333.
Kimmel, C. B., Ballard, W. W., Kimmel, S. R., Ullmann, B. and Schilling, T. F. (1995). Stages of embryonic development of the zebrafish. *Dev. Dyn.* **203**, 253-310.
Kofler, N. M., Cuervo, H., Uh, M. K., Murtomaki, A. and Kitajewski, J. (2015). Combined deficiency of Notch1 and Notch3 causes pericyte dysfunction, models CADASIL, and results in arteriovenous malformations. *Sci. Rep.* **5**, 16449.
Kok, F. O., Shin, M., Ni, C.-W., Gupta, A., Grosse, A. S., van Impel, A., Kirchmaier, B. C., Peterson-Maduro, J., Kourkoulis, G., Male, I. et al. (2015). Reverse genetic screening reveals poor correlation between morpholino-induced and mutant phenotypes in zebrafish. *Dev. Cell* **32**, 97-108.
Krymskaya, V. P., Hoffman, R., Eszterhas, A., Ciocca, V. and Panettieri, R. A. Jr (1997). TGF-beta 1 modulates EGF-stimulated phosphatidylinositol 3-kinase activity in human airway smooth muscle cells. *Am. J. Physiol.* **273**, L1220-L1227.
Kucenas, S., Takada, N., Park, H.-C., Woodruff, E., Broadie, K. and Appel, B. (2008). CNS-derived glia ensheath peripheral nerves and mediate motor root development. *Nat. Neurosci.* **11**, 143-151.
Lee, C.-W., Lin, C.-C., Lin, W.-N., Liang, K.-C., Luo, S.-F., Wu, C.-B., Wang, S.-W. and Yang, C.-M. (2007). TNF-alpha induces MMP-9 expression via activation of Src/EGFR, PDGFR/PI3K/Akt cascade and promotion of NF-kappaB/p300 binding in human tracheal smooth muscle cells. *Am. J. Physiol. Lung Cell. Mol. Physiol.* **292**, L799-L812.
Lee, R. T. H., Knapik, E. W., Thiery, J. P. and Carney, T. J. (2013). An exclusively mesodermal origin of fin mesenchyme demonstrates that zebrafish trunk neural crest does not generate ectomesenchyme. *Development* **140**, 2923-2932.
Lehti, K., Allen, E., Birkedal-Hansen, H., Holmbeck, K., Miyake, Y., Chun, T.-H. and Weiss, S. J. (2005). An MT1-MMP-PDGF receptor-beta axis regulates mural cell investment of the microvasculature. *Genes Dev.* **19**, 979-991.
Lindahl, P., Johansson, B. R., Leveen, P. and Betsholtz, C. (1997). Pericyte loss and microaneurysm formation in PDGF-B-deficient mice. *Science* **277**, 242-245.
Lindblom, P., Gerhardt, H., Liebner, S., Abramsson, A., Enge, M., Hellstrom, M., Backstrom, G., Fredriksson, S., Landegren, U., Nyström, H. C. et al. (2003). Endothelial PDGF-B retention is required for proper investment of pericytes in the microvessel wall. *Genes Dev.* **17**, 1835-1840.
Majesky, M. W. (2007). Developmental basis of vascular smooth muscle diversity. *Arterioscler. Thromb. Vasc. Biol.* **27**, 1248-1258.
Mascall, K. S., Small, G. R., Gibson, G. and Nixon, G. F. (2012). Sphingosine-1-phosphate-induced release of TIMP-2 from vascular smooth muscle cells inhibits angiogenesis. *J. Cell Sci.* **125**, 2267-2275.
Miano, J. M., Georger, M. A., Rich, A. and De Mesy Bentley, K. L. (2006). Ultrastructure of zebrafish dorsal aortic cells. *Zebrafish* **3**, 455-463.
Owens, G. K. (1995). Regulation of differentiation of vascular smooth muscle cells. *Physiol. Rev.* **75**, 487-517.
Perkins, M. E., Ji, T. H. and Hynes, R. O. (1979). Cross-linking of fibronectin to sulfated proteoglycans at the cell surface. *Cell* **16**, 941-952.
Pitrone, P. G., Schindelin, J., Stuyvenberg, L., Preibisch, S., Weber, M., Eliceiri, K. W., Huisken, J. and Tomancak, P. (2013). OpenSPIM: an open-access light-sheet microscopy platform. *Nat. Methods* **10**, 598-599.
Pouget, C., Pottin, K. and Jaffredo, T. (2008). Sclerotomal origin of vascular smooth muscle cells and pericytes in the embryo. *Dev. Biol.* **315**, 437-447.
Rossi, A., Kontarakis, Z., Gerri, C., Nolte, H., Hölper, S., Krüger, M. and Stainier, D. Y. R. (2015). Genetic compensation induced by deleterious mutations but not gene knockdowns. *Nature* **524**, 230-233.
Sanjana, N. E., Cong, L., Zhou, Y., Cunniff, M. M., Feng, G. and Zhang, F. (2012). A transcription activator-like effector toolbox for genome engineering. *Nat. Protoc.* **7**, 171-192.
Santoro, M. M., Pesce, G. and Stainier, D. Y. (2009). Characterization of vascular mural cells during zebrafish development. *Mech. Dev.* **126**, 638-649.
Saunders, W. B., Bohnsack, B. L., Faske, J. B., Anthis, N. J., Bayless, K. J., Hirschi, K. K. and Davis, G. E. (2006). Coregulation of vascular tube stabilization by endothelial cell TIMP-2 and pericyte TIMP-3. *J. Cell Biol.* **175**, 179-191.
Scheer, N. and Campos-Ortega, J. A. (1999). Use of the Gal4-UAS technique for targeted gene expression in the zebrafish. *Mech. Dev.* **80**, 153-158.
Seiler, C., Abrams, J. and Pack, M. (2010). Characterization of zebrafish intestinal smooth muscle development using a novel sm22alpha-b promoter. *Dev. Dyn.* **239**, 2806-2812.
Smola, H., Stark, H.-J., Thiekötter, G., Mirancea, N., Krieg, T. and Fusenig, N. E. (1998). Dynamics of basement membrane formation by keratinocyte-fibroblast interactions in organotypic skin culture. *Exp. Cell Res.* **239**, 399-410.
Stratman, A. N. and Davis, G. E. (2012). Endothelial cell-pericyte interactions stimulate basement membrane matrix assembly: influence on vascular tube remodeling, maturation, and stabilization. *Microsc. Microanal.* **18**, 68-80.
Stratman, A. N., Malotte, K. M., Mahan, R. D., Davis, M. J. and Davis, G. E. (2009). Pericyte recruitment during vasculogenic tube assembly stimulates endothelial basement membrane matrix formation. *Blood* **114**, 5091-5101.
Stratman, A. N., Schwindt, A. E., Malotte, K. M. and Davis, G. E. (2010). Endothelial-derived PDGF-BB and HB-EGF coordinately regulate pericyte recruitment during vasculogenic tube assembly and stabilization. *Blood* **116**, 4720-4730.
Vanhollebeke, B., Stone, O. A., Bostaille, N., Cho, C., Zhou, Y., Maquet, E., Gauquier, A., Cabochette, P., Fukuhara, S., Mochizuki, N. et al. (2015). Tip cell-specific requirement for an atypical Gpr124- and Reck-dependent Wnt/beta-catenin pathway during brain angiogenesis. *Elife* **4**, 1-25.
Wang, Q., Zhao, N., Kennard, S. and Lilly, B. (2012). Notch2 and Notch3 function together to regulate vascular smooth muscle development. *PLoS ONE* **7**, e37365.
Wang, Y., Pan, L., Moens, C. B. and Appel, B. (2014). Notch3 establishes brain vascular integrity by regulating pericyte number. *Development* **141**, 307-317.
Wasteson, P., Johansson, B. R., Jukkola, T., Breuer, S., Akyurek, L. M., Partanen, J. and Lindahl, P. (2008). Developmental origin of smooth muscle cells in the descending aorta in mice. *Development* **135**, 1823-1832.
Westerfield, M. (1995). *The Zebrafish Book*. Eugene, OR: University of Oregon Press.
Whitesell, T. R., Kennedy, R. M., Carter, A. D., Rollins, E.-L., Georgijevic, S., Santoro, M. M. and Childs, S. J. (2014). An alpha-smooth muscle actin (acta2/alphasma) zebrafish transgenic line marking vascular mural cells and visceral smooth muscle cells. *PLoS ONE* **9**, e90590.
Wiegreffe, C., Christ, B., Huang, R. and Scaal, M. (2007). Sclerotomal origin of smooth muscle cells in the wall of the avian dorsal aorta. *Dev. Dyn.* **236**, 2578-2585.
Wiens, K. M., Lee, H. L., Shimada, H., Metcalf, A. E., Chao, M. Y. and Lien, C.-L. (2010). Platelet-derived growth factor receptor beta is critical for zebrafish intersegmental vessel formation. *PLoS ONE* **5**, e11324.
Yang, X.-Y., Yao, J.-H., Cheng, L., Wei, D.-W., Xue, J.-L. and Lu, D.-R. (2003). Molecular cloning and expression of a smooth muscle-specific gene SM22alpha in zebrafish. *Biochem. Biophys. Res. Commun.* **312**, 741-746.
Yao, Y., Chen, Z. L., Norris, E. H. and Strickland, S. (2014). Astrocytic laminin regulates pericyte differentiation and maintains blood brain barrier integrity. *Nat. Commun.* **5**, 3413.
Yasutake, J., Inohaya, K. and Kudo, A. (2004). Twist functions in vertebral column formation in medaka, Oryzias latipes. *Mech. Dev.* **121**, 883-894.

Development (2017) 144, 115-127 doi:10.1242/dev.143131

Yeo, G. H., Cheah, F. S. H., Winkler, C., Jabs, E. W., Venkatesh, B. and Chong, S. S. (2009). Phylogenetic and evolutionary relationships and developmental expression patterns of the zebrafish twist gene family. *Dev. Genes Evol.* **219**, 289-300.

Yurchenco, P. D. (2011). Basement membranes: cell scaffoldings and signaling platforms. *Cold Spring Harb Perspect. Biol.* **3**, a004911.

Zaucker, A., Mercurio, S., Sternheim, N., Talbot, W. S. and Marlow, F. L. (2013). notch3 is essential for oligodendrocyte development and vascular integrity in zebrafish. *Dis. Model. Mech.* **6**, 1246-1259.

Zhao, N., Koenig, S. N., Trask, A. J., Lin, C.-H., Hans, C. P., Garg, V. and Lilly, B. (2015). MicroRNA miR145 regulates TGFBR2 expression and matrix synthesis in vascular smooth muscle cells. *Circ. Res.* **116**, 23-34.

SUPPLEMENTARY MATERIAL

Stratman et al., Supplemental Figure 1

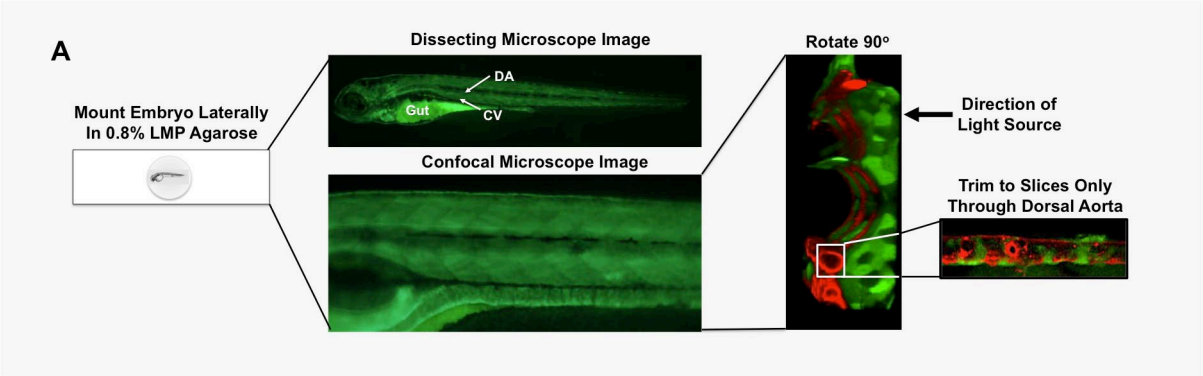

Supplementary Figure 1. Mounting and imaging strategy of mural cell transgenic lines. (**A**) Embryos were mounted in 0.9% low melt point (LMP) agarose at the desired time point of imaging. Confocal stacks were acquired through the zebrafish at a 1.5 μM step size. Typically due to limitations of penetrance of lasers with confocal microscopy, one side of the embryo (the side closest to the light source) is imaged in greater detail. Excess slices from imaging are trimmed to only include the slices that include the dorsal aorta. It is key for trimming for the embryo to have been mounted as flat as possible.

Stratman et al., Supplemental Figure 2

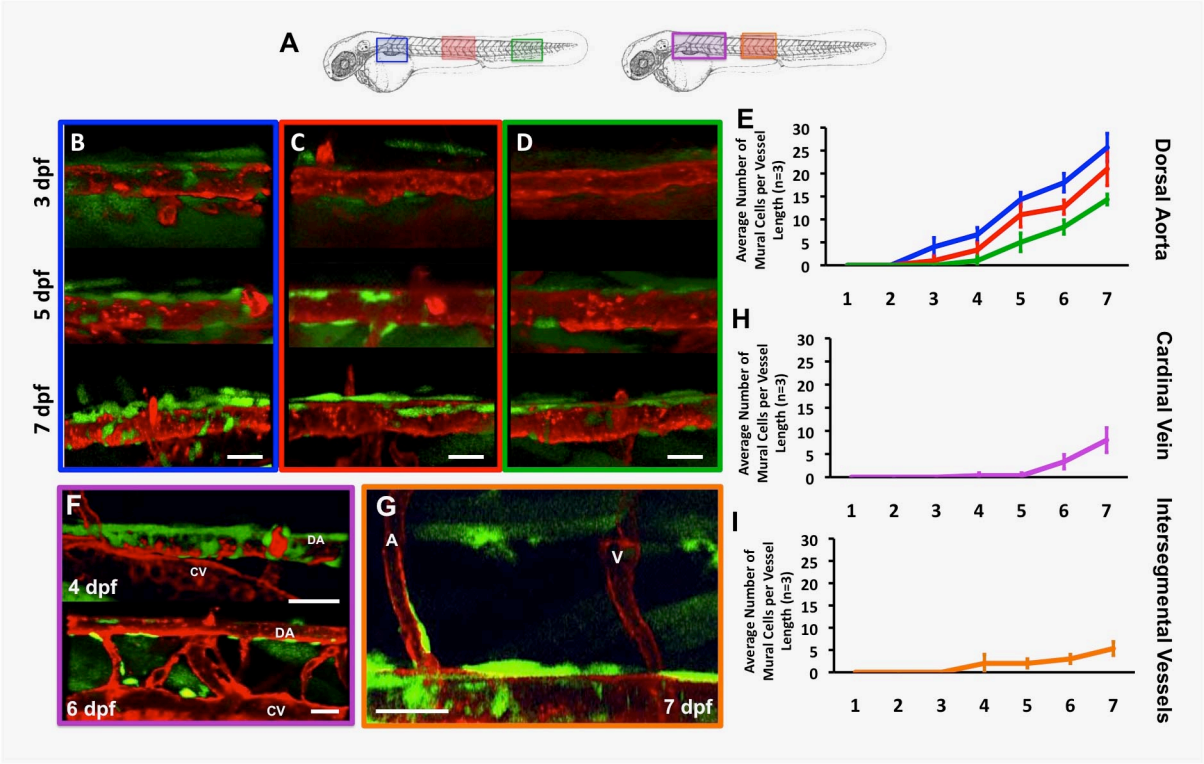

Supplementary Figure 2. Time-course analysis and quantification of mural cell accumulation in different vascular beds. (**A**) Schematic representation of areas assessed for mural cell accumulation over time in the developing zebrafish. (**B-E**) Representative images of mural cell association with the dorsal aorta in sections proximal to the head (B, blue boxes and lines), mid-trunk (C, red boxes and lines), and in the tail region (D, green boxes and lines) at 3, 5 and 7 dpf. (E) Quantification of the number of mural cells associated with a four-somite length of dorsal aorta over time. Blue line is the quantification from the most proximal section to the head, red line is the quantification from mid-trunk section and the green line is quantification from the more distal tail region. (**F,H**) Representative images of mural cells associated with the cardinal vein at 4 and 6 dpf (F, purple boxes and lines), and quantification of the number of mural cells associated with a four-somite length of cardinal vein over time (H). (**G,I**) Representative image of mural cells associated with the intersegmental arteries at 7 dpf (G, orange boxes and lines), and quantification of the number of mural cells associated with a four-ISV length of the zebrafish trunk over time (I). Scale bars = 50 µm. Mean ± s.e.m. n=5 fish per region.

Stratman et al., Supplemental Figure 3

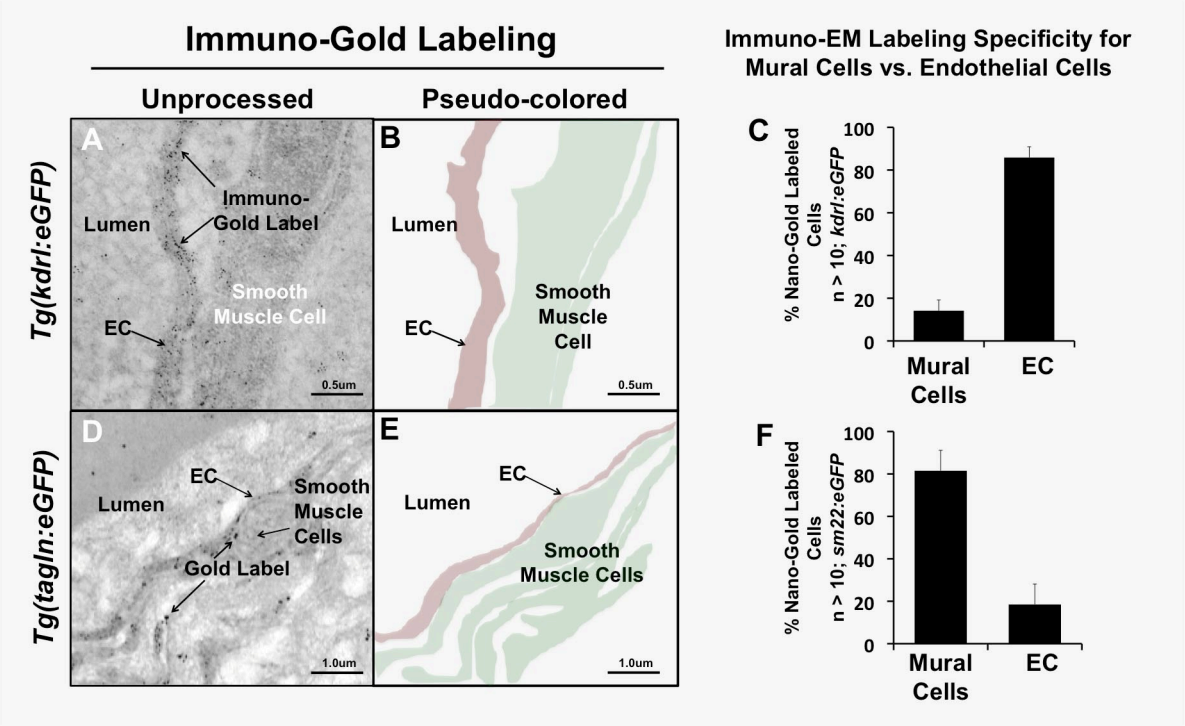

Supplementary Figure 3. Immuno-EM confirms specificity of the *tagln* mural cell transgenic line. **(A-C)** Immuno-gold labeling of GFP of the *Tg(kdrl:egfp)* line shows specific labeling of the endothelium. (A) Low magnification and pseudo-colored interpretation of the endothelial (red) immuno-gold labeling. (B) Higher magnification of the endothelium shows more clearly the immuno-gold label. (C) Quantification of the number of immuno-gold labeled sites, showing that the labeling was largely endothelial specific. (**D-F**) Immuno-gold labeling of GFP of the *Tg(tagln:egfp)* line shows specific labeling of mural cells. (D) Low magnification and pseudo-colored interpretation of the mural cell (green) immuno-gold labeling. (E) Higher magnification of the mural cells shows more clearly the immuno-gold label outside of the endothelial cells lining the dorsal aorta. (F) Quantification of the number of immuno-gold labeled sites, showing that the labeling was largely mural cell specific. n = 10 image regions measured, regions collected from 2-3 individual fish. Scale bars = 0.5 or 1.0 μm as indicated. Mean ± s.e.m.

Stratman et al., Supplemental Figure 4

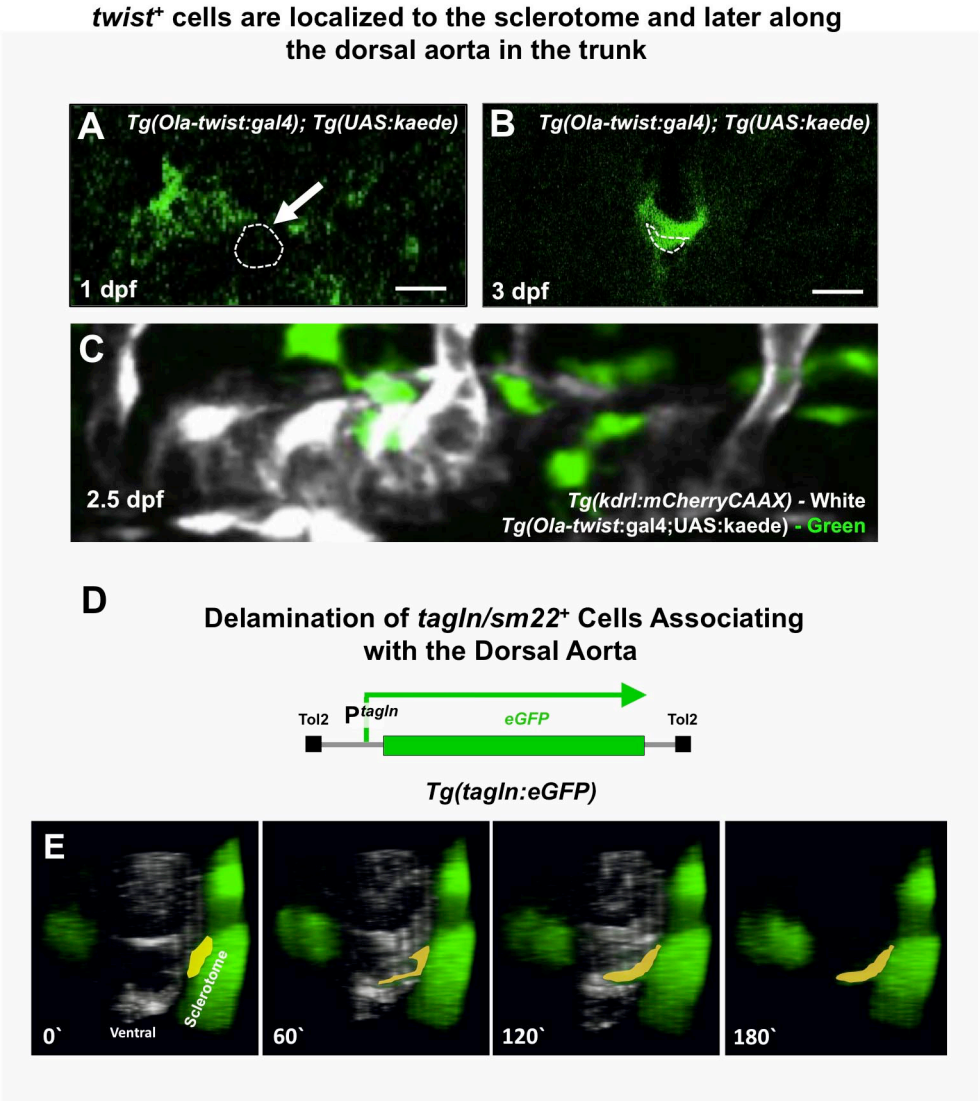

Supplementary Figure 4. Expression and distribution of *twist1*+ cells during development coincides with delamination of *tagln/sm22*+ membrane from the sclerotome. (**A,B**) Confocal transverse view images of green unconverted kaede fluorescence in the mid-trunk of *Tg(Ola-twist:gal4), Tg(uas:kaede)* animals at 1 dpf (A) and 3 dpf (B). Twist+ cells are initially found in the sclerotome region of the somites (A), but later become concentrated around the vicinity of the dorsal aorta (B). Representative images were obtained from n = 3-5 fish; 2 rounds of immunostaining. (**C**) Confocal lateral view images of unconverted kaede (green) on a red fluorescent dorsal aorta (white) of a *Tg(Ola-twist:gal4), Tg(uas:kaede), Tg(kdrl:mCherryCAAX)* triple transgenic animal at 2.5 dpf. Images were obtained from 5 fish, from 2 separate experiments and a representative image chosen. (**D**) Schematic diagram of the *Tg(tagln:egfp)* transgene, with the *transgelin (tagln)* promoter driving expression of egfp in the cytoplasm. (**E**) Selected frames from a confocal time-lapse image series collected from a *Tg(tagln:egfp)* (in green); *Tg(kdrl:mCherryCAAX)* (in white) double-transgenic fish shows the movement of a *tagln*+ membrane (yellow) from the adjacent sclerotome delaminate and associate with the dorsal aorta. The image reconstructions shown are tilted ventral views, looking at a 45^{o} upward tilted angle along the length of the dorsal aorta. Confocal images were acquired every 10 minutes and the displayed stills are shown at approximately 1-hour intervals. Scale bars = 50 μm. In total, 13 *tagln*+ cells investing the DA were traced to the sclerotome in 6 independent time-lapse experiments.

Stratman et al., Supplemental Figure 5

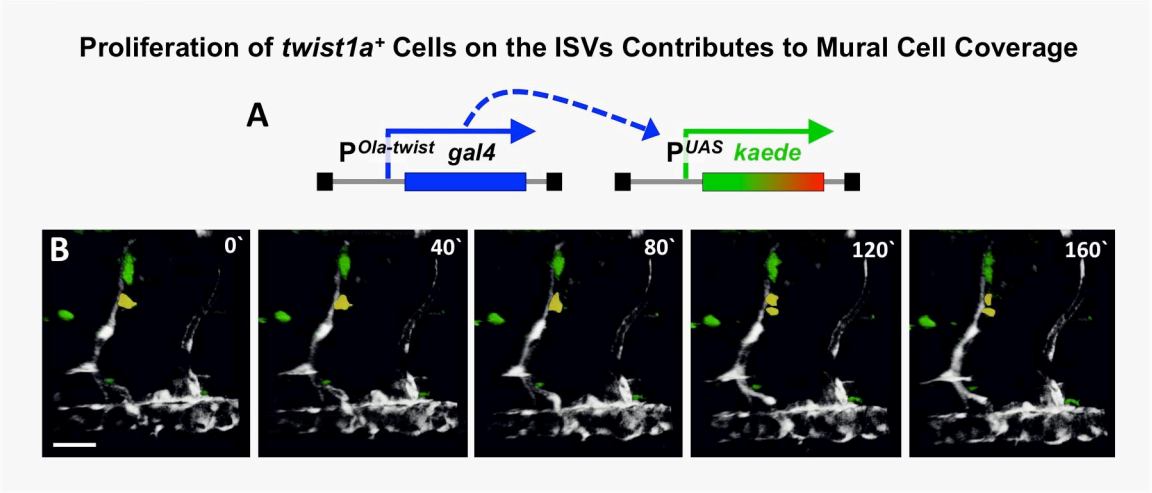

Supplementary Figure 5. ***twist1+*** **cells proliferate to contribute to mural cell coverage.** (**A**) Schematic diagram of the transgenes in *Tg(Ola-twist:gal4), Tg(uas:kaede)* double transgenic fish, in which the Medaka (*Oryzias latipes) twist* promoter (Ola-twist) is used to drive expression of Gal4 from the *Ola-twist:gal4* transgene, which then activates expression of green to red photoconvertible Kaede from the *uas:kaede* transgene. (B) Selected frames from a confocal time-lapse image series collected from a 2-2.5 dpf *Tg(Ola-twist:gal4), Tg(uas:kaede)* double-transgenic fish. Two *twist1+* ISV-associated cells highlighted in yellow and green undergo cell division over the course of the time-lapse imaging experiment. The image reconstructions shown are lateral views of the mid-trunk, with rostral to the left. Confocal images were acquired every 10 minutes and the displayed stills are shown at approximately 40-minute intervals. Scale bars = 50 μm. Still images are representative of data collected from 3 individual time-lapse experiments.

Stratman et al., Supplemental Figure 6

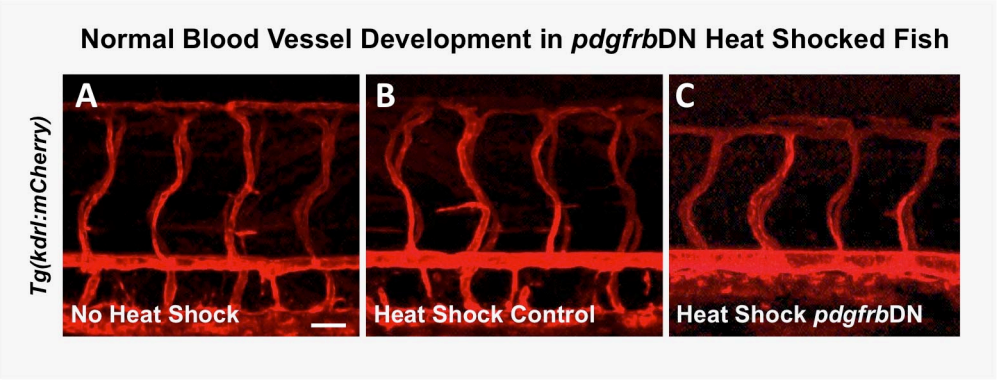

Supplementary Figure 6. Activation of the *pdgfrDN* construct starting at 1 dpf does not lead to gross defects in vascular patterning. Confocal images of 5 dpf non-heat shocked triple transgenic *Tg(kdrl:mCherry); Tg(hsp70:gal4); Tg(uas:pdgfrbdn-yfp)* animals (**A**), heat shocked control *Tg(kdrl:mCherry); Tg(hsp70:gal4)* animals (**B**), or heat-shocked *pdgfrbDN*-expressing triple transgenic *Tg(kdrl:mCherry); Tg(HSP70:gal4; UAS:pdgfrbDN-YFP)* animals (**C**). Animals demonstrate no gross vascular patterning defects from either the heat shock process or activation of the *pdgfrDN* construct. Scale bars = 50 μm. n= 5 fish.

Stratman et al., Supplemental Figure 7

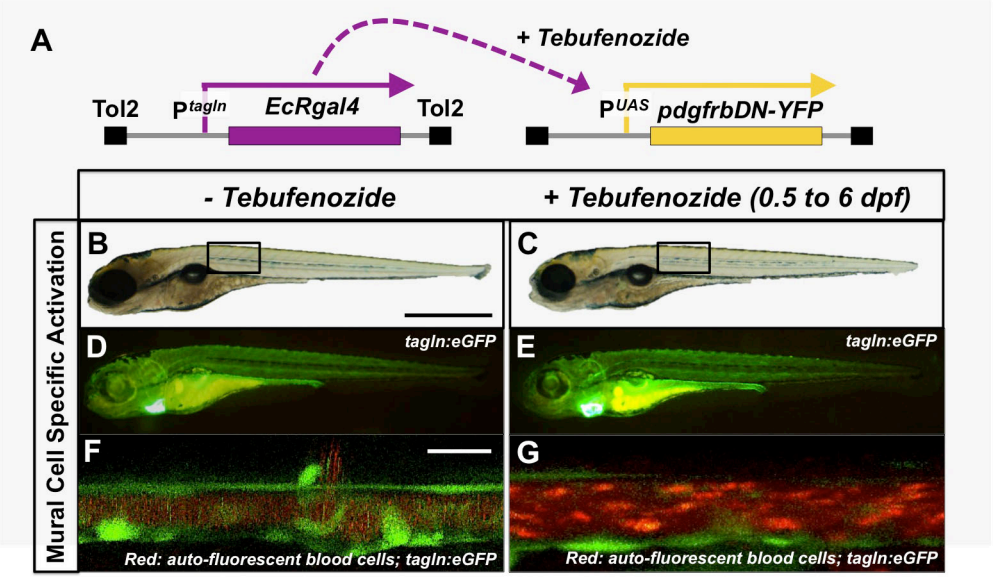

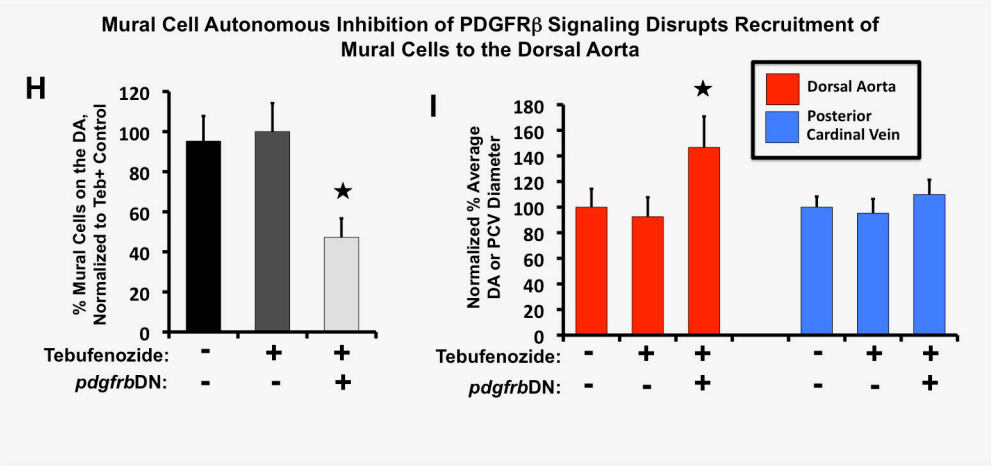

Supplementary Figure 7. Mural cell-autonomous inhibition of *pdgfr* signaling leads to loss of mural cell coverage on the zebrafish dorsal aorta. (**A**) Schematic diagram showing the *Tg(tagln:EcRgal4)* and *Tg(uas:pdgfrbDN-YFP)* transgenes used for heat shock-inducible expression of dominant negative PDGF receptor beta (*pdgfrbDN*). These fish were outcrossed to *Tg(tagln:egfp)* transgenic fish to generate triple heterozygotes, treated with tebufenozide for the indicated time frame, and imaged for analysis of mural cell coverage at 6 dpf. (**B-G**) Representative 6dpf images of untreated (B,D,F) or 0.5-6 dpf tebufenozide-treated (C,E,G) *Tg(tagln:egfp)*, *Tg(tagln:EcRgal4)*, *Tg(uas:pdgfrbDN-YFP)* triple-transgenic animals. Images show whole-animal transmitted light images (B,C), whole-animal green epifluorescence images of *tagln:egfp* green fluorescence (D,E), and higher-magnification confocal images of the dorsal aorta, showing green fluorescent EGFP-positive vSMC and red autofluorescent circulating red blood cells marking the vascular compartment (F,G). (**H**) Quantification of the percent number of mural cells covering the dorsal aorta with or without tebufenozide treatment and

activation of dominant-negative *pdgfrbDN*. Fish were treated with the chemical as described above, imaged at 6 dpf and the number of *tagln/sm22*$^{+}$ cells per three-somite segment length of dorsal aorta counted. The data represent the % number of *tagln/sm22*$^{+}$ cells normalized to the control tebufenozide-treated condition (second column). n= 5 fish from a single experiment; 2 experimental replicates, 2 independent fish clutches per experiment. In more absolute values, we typically see approximately 20 ± s.e.m vSMCs recruit to a 3 somite segment of dorsal aorta under control conditions, and approximately 9-10 ± s.e.m vSMCs recruit to a 3 somite length of dorsal aorta under "DN" activation conditions. (I) Quantification of dorsal aorta (left columns, red) and posterior cardinal vein (right columns, blue) diameter, demonstrating markedly larger dorsal aorta in tebufenozide-treated *Tg(tagln:egfp)*, *Tg(tagln:EcRgal4)*, *UAS:pdgfrbDN-YFP)* triple-transgenic animals expressing *pdgfrbDN* autonomously in mural cells. No significant effects were noted on the diameter of the cardinal vein. 3-5 fish were measured per sample, with 10 separate dorsal aorta measurements per fish; experiment repeated twice with consistent results. Values were normalized to the *tagln/sm22*$^{+}$ cell counts from non-tebufenozide-treated control fish (column 1). Mean ± s.e.m.; * = $p \leq 0.05$ significance from control. Scale bars = 1 mm for B,C and 50 µm for F,G.

Stratman et al., Supplemental Figure 8

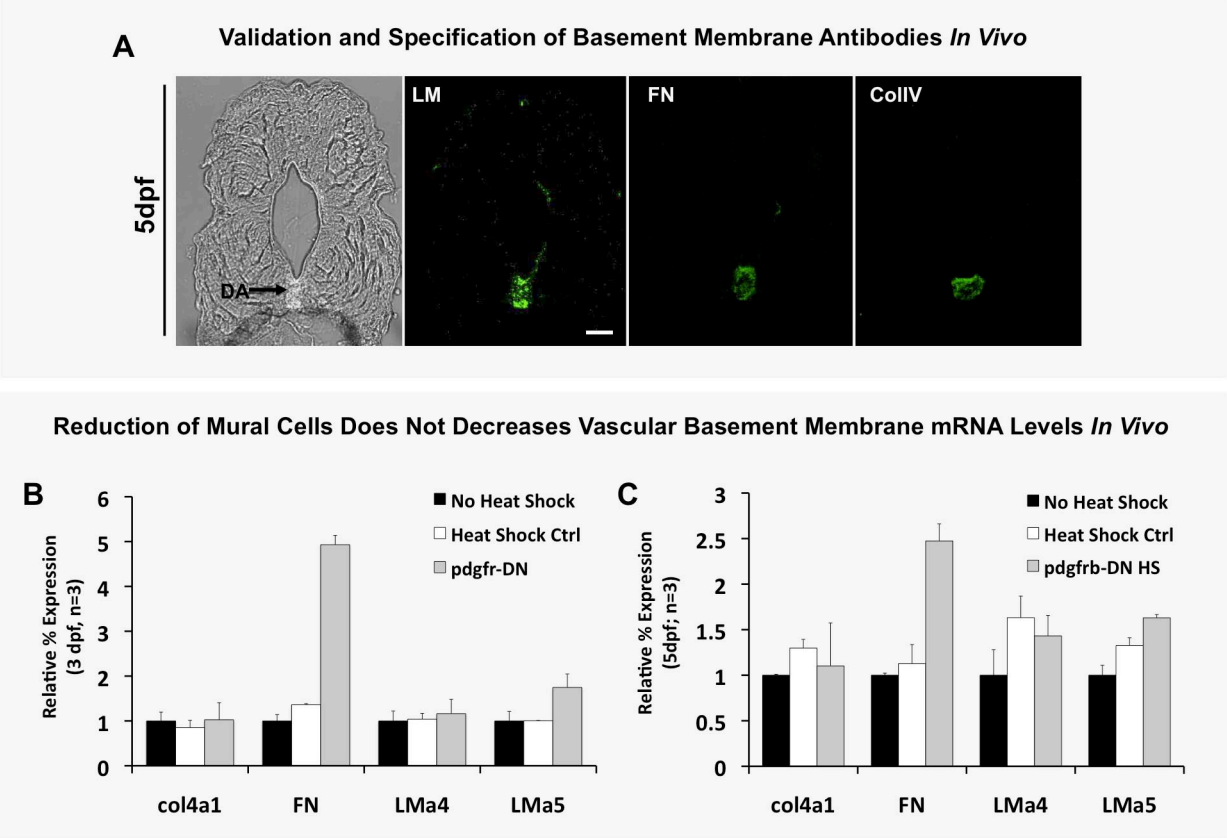

Supplementary Figure 8. mRNA transcript levels of individual basement membrane components are not reduced. (**A**) Validation and demonstration of the antibodies utilized to show vascular enrichment of the basement membrane proteins analyzed throughout the manuscript. (**B,C**) qPCR analysis of mRNA transcript levels of individual basement membrane components. Fish were heat shocked starting at 1 dpf and collected at 3 dpf (B) and 5 dpf (C) for analysis. Data are normalized to ef1α and to no-heat shock controls (black columns). Data represents RNA collected from 15 pooled embryos. qPCR repeated in triplicate twice per sample, with 2 experimental replicates showing consistent results. Scale bars = 50 μm. Mean ± s.d.

Stratman et al., Supplemental Figure 9

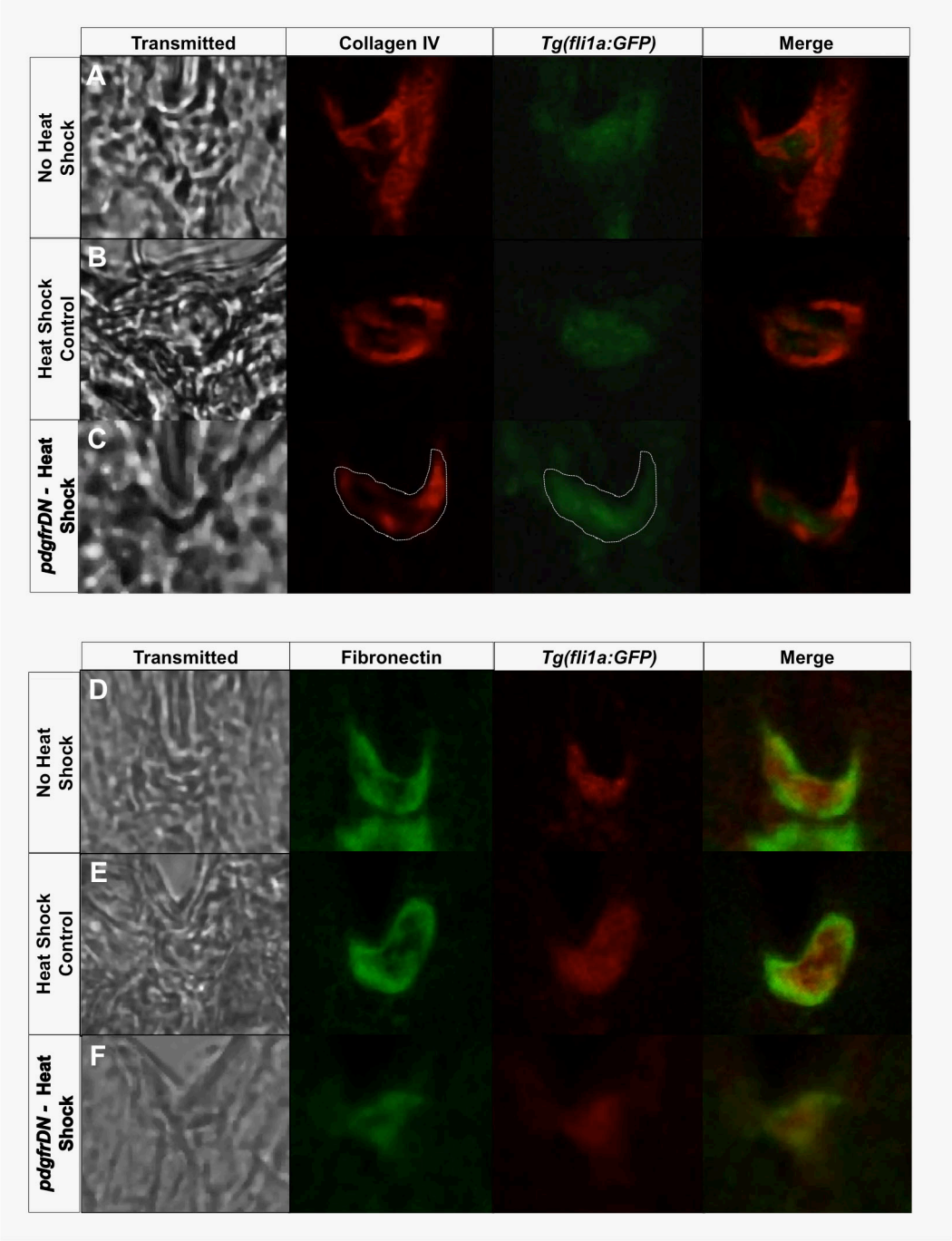

Supplementary Figure 9. Co-staining of vascular and basement membrane proteins shows vascular enrichment. (**A-C**) Collagen IV with vascular co-immunostaining: column 1- transmitted light image of the region of interest; column 2- collagen IV immunolabeling (pseudocolored red); column 3- immunolabeling of GFP expressed by the Tg(fli1a:GFP) zebrafish line (pseudocolored green); column 4- merge of the collagen IV and vascular images. Three conditions were analyzed: No Heat Shock Controls (A), Heat Shock Controls (B), and *pdgfrDN*- Heat Shock (C). (**D-F**) Fibronectin with vascular co-immunostaining: column 1- transmitted light image of the region of interest; column 2- fibronectin immunolabeling (pseudocolored green); column 3- immunolabeling of GFP expressed by the *Tg(fli1a:GFP)* zebrafish line (pseudocolored red); column 4- merge of the collagen IV and vascular images. Three conditions were analyzed: No Heat Shock Controls (D), Heat Shock Controls (E), and *pdgfrDN*- Heat Shock (F). Representative images were chosed from 3 independent rounds of immunostaining.

SUPPLEMENTARY MOVIES

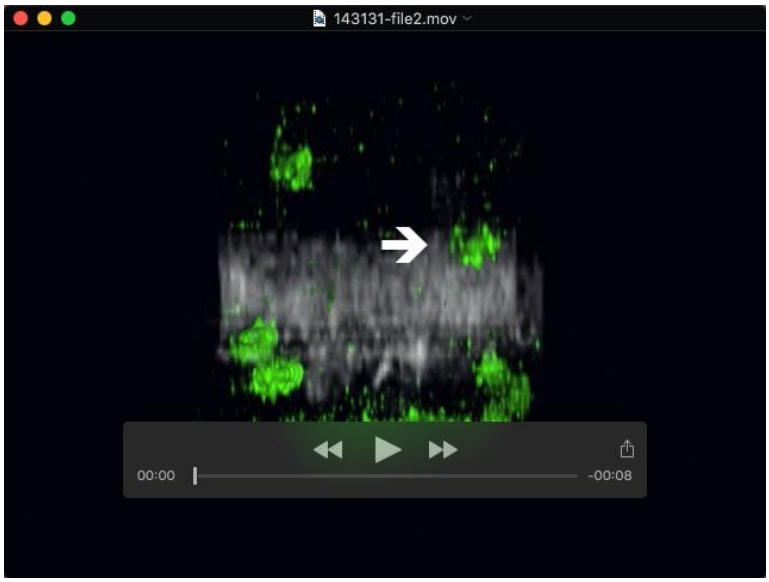

Movie 1. Nuclear tracking of *Tg(tagln:nlsgfp-2a-cfp-f)* mural cells. Confocal time-lapse movie from a *Tg(tagln:nlsgfp-2a-cfp-f), Tg(kdrl:mCherryCAAX)* double-transgenic fish shows the movement of a *tagln*+ nucleus (green) from the adjacent sclerotome underneath the dorsal aorta (white), taking up position adjacent to the aorta on the opposite side of the trunk midline. The image reconstructions shown are ventral views, with rostral to the right. Confocal images were acquired every 10 minutes starting at approximately 2.5 dpf.

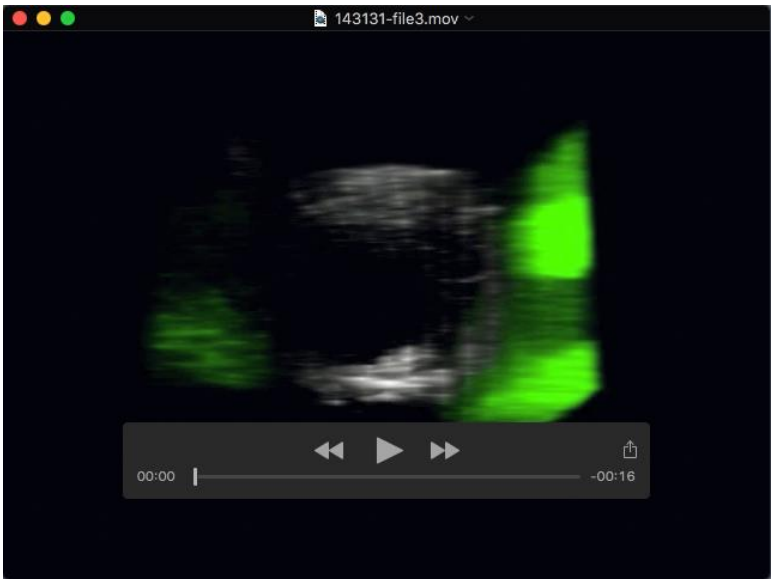

Movie 2. Imaging of *Tg(tagln:egfp)* bulk membrane transport from the sclerotome to associate with the dorsal aorta. Confocal time-lapse movie from a *Tg(tagln:egfp), Tg(kdrl:mCherryCAAX)* double-transgenic fish shows the movement of *tagln*+ membrane (green) from the adjacent sclerotome toward the dorsal aorta (red). The image reconstruction shows the vessel in transverse view. Confocal images were acquired every 10 minutes starting at approximately 2.5 dpf.

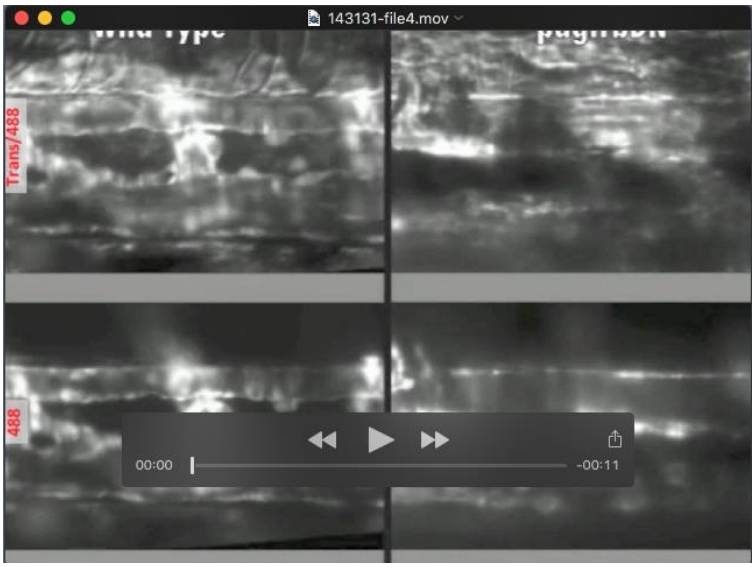

Movie 3. SPIM imaging of *pdgfrbdn* mural cell disrupted animals reveals increased vessel elasticity. SPIM imaging of *Tg(fli1:egfp)^{y1}; Tg(hsp70:gal4); Tg(uas:pdgfrbDN-YFP)* animals (right, top and bottom) versus control *Tg(fli1:egfp)^{y1}; Tg(hsp70:gal4)* heat shocked siblings (left, top and bottom). Images on top were acquired with transmitted light, demonstrating normal blood flow in both conditions. Images on the bottom are acquired using a 488 nm laser to visualize GFP-positive endothelium, demonstrating increased vessel elasticity in PDGFRB-DN expressing animals.

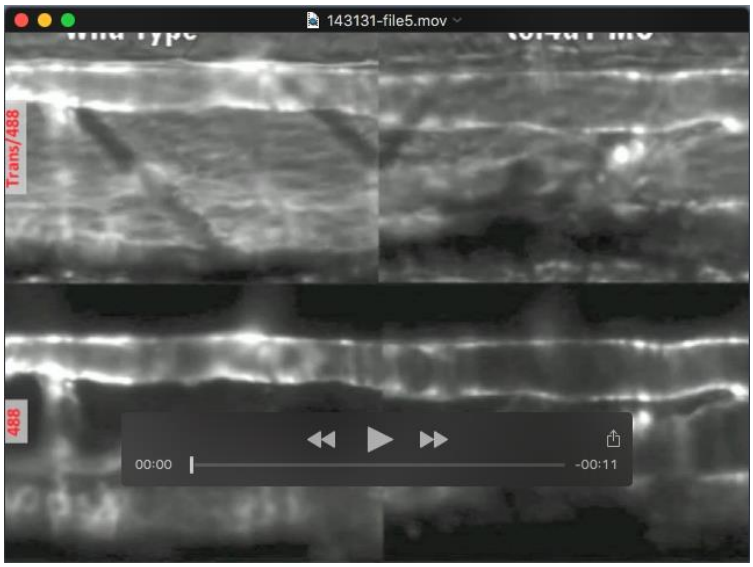

Movie 4. SPIM imaging of *col4a1* MO treated animals reveals increased vessel elasticity. SPIM imaging of *Tg(fli1:egfp)*^{y1} *col4a1* MO injected animals (right, top and bottom) versus WT control siblings (left, top and bottom). Images on top were acquired with transmitted light, demonstrating normal blood flow in both conditions; images on the bottom were acquired using a 488 nm laser to visualize GFP-positive endothelium, demonstrating increased vessel elasticity in *col4a1* morpholino-injected animals.

SUPPLEMENTARY METHODS

Previously Published Zebrafish Transgenic Lines Utilized

The Tg(*fli1a:EGFP*)^{y1}; Tg(*kdrl:mCherry-CAAX*)^{y171}; Tg(*tagln:egfp*)^{p151}; Tg(-1.5*hsp70I:gal4*)^{kca4}; Tg(*UAS:pdgfrDN-YFP*)^{sr1} maintained and screened based on YFP expression from the DN construct; Tg(*Ola-Twist:gal4*)^{sq11}; Tg(*UAS:kaede*)^{rk8} are all previously published.

Generation and Genotyping of *col4a1*^{st93} Allele

TALE binding sites were identified in the *col4a1* genomic sequence using the TALE-NT 2.0 tool (Cermak et al. 2011; Doyle et al. 2013). pCS2+ vectors expressing TALENs targeting the following sequences were cloned: 5'-TTTTCTGTCAGGGTCTTC-3' and 5'-GGGATTCCTTGAGGTCCA-3'. Expression vectors were linearized with SmaI and transcribed *in vitro* using the mMessage mMachine® T7 Ultra Kit (Ambion). A mixture containing equal amounts of each mRNA (~400pg each) was injected into one-cell stage zebrafish embryos. On the next day, some surviving injected embryos were lysed and genotyped following the protocols below to measure the efficiency of inducing genomic deletions. The remaining fish were raised to adulthood, and mosaic carriers were identified by assaying for transmission of genomic deletions to their progeny.

col4a1$^{st93/st93}$ mutants were genotyped using the primers: Fw: 5`-TGAATTTCCGGAGAAACCATTA- 3`; Rv: 5`- AAAATGAGTCATACCGGTG GTC-3`; followed by restriction digest with the enzyme Hpy188III (NEB) for 2 hours.

Morpholino Injections

Morpholino injections were performed on the zebrafish embryos at the 1-4 cell stage using a microinjector. Doses were determined by titration of morpholinos to levels that produced maximal vascular-defects with minimal to no nonspecific toxic effects. Only fish with overtly normal morphology were chosen for analysis within studies.

TEM and Immuno-EM

Ultra-thin sections (90nm) were produced using a Reichert-Jung UltraCut E ultramicrotome. The sections were transferred to Formvar Carbon-Coated Nickel grids (Electron Microscopy Sciences, Hatfield, PA). Sections were rinsed in PBS, incubated in 1% Normal Goat Serum (NGS) made in PBS, incubated in primary antibody (rabbit anti-

GFP) 1:50 overnight at 4C. Next, sections were rinsed in 1% NGS, incubated in secondary antibody 1:100 Nanogold (anti-rabbit IgG) (Nanoprobes, Yaphank, NY). The sections were then rinsed in PBS, postfixed with 1% glutaraldehyde and rinsed in DDW. Finally, the Nanogold was silver enhanced using HQ Silver (Nanoprobes, Yaphank, NY) for four minutes at room temperature in the dark. Grids were then rinsed in DDW and post-stained with uranyl acetate and lead citrate and examined in a JEOL 1400 transmission electron microscope operating at 80kV. Negative controls (minus primary antibody) were performed in parallel to experimental sections, where only the secondary antibody was used.

Heat Shock and EcRgal4 driven *pdgfrbDN* activation treatments

For heat shock treated embryos: embryos were placed as pairs into 96 well PCR plates. The following heat shock program was run: 1) 38°C, 15 min; 2) 28°C, 45 min; 3) GoTo step 1 11x; 4) Hold at 28°C. Embryos were removed from the PCR plate daily and allowed approximately 8-12 hours of free motility between rounds of heat shock.

Cell Culture Assays

3-dimensional (3D) collagen type I in vitro assays were done essentially as described ((Stratman et al. 2009)), utilizing 2.5mg/mL collagen type I (BD Biosciences, Acid Extracted) gels including SCF (R&D Systems, #255-SC/CF), SDF1a (R&D Systems, 350,NS/CF), IL3 (R&D Systems, #203-IL/CF) and FGF (R&D Systems, #233-FB-025/CF) in the gel at 200ng/mL. HUVECs were seeded within the collagen gel at $2x10^6$ cells per mL and pericytes at 20% the HUVEC density. Culture media for the assays contained ascorbic acid, FGF and IGF-II (R&D Systems, #292-G2-250). Assays were fixed in 2% paraformaldehyde (PFA) at 5 days and processed for future analysis.

Immunostaining and Western blot analysis

Tissue sections and 3D collagen were immunostained following the same basic protocol: 1) 30 min RT incubation in Tris-Glycine; 2) 1hr RT incubation +/- permeabilization with 0.01% TritonX-100; 3) 2hr RT incubation in blocking solution (5% Sheep Serum, 1% Roche Blocking Buffer in PBST); 4) 1hr at RT - over night 4°C incubation with 1:1000 primary antibody; 5) wash with PBST; 6) 2-3hr RT incubation with 1:2000 secondary

antibody in 5% Sheep Serum, 1% Roche Blocking Buffer in PBST; 7) wash with PBST and imaging analysis. Quantification of immunostaining intensity was performed by ImageJ analysis software. Images were acquired using a Leica SP5 II confocal microscope. All images were acquired at the same intensity, step size and image resolution for analysis. Data is reported as the percent average intensity per region of interest size from a minimum of 3 images from 3 independent experiments ± s.e.m.

Secondary HRP-conjugated antibodies were purchased from Santa Cruz and used at 1:2000 in 5% milk. Primary antibodies are described in the 'Reagents' section and used at 1:1000. Quantification of relative band density was performed using ImageJ software. Data is reported as the percent average density from a minimum of 2-3 blots from at least 2 independent experiments ± s.e.m.

qPCR Primer Sets

Primer sets are as follows: ef1a: FW- 5`- CTGGAGGCCAGCTCAAACAT- 3` RV- 5`-ATCAAGAAGAGTAGTACCGCTAGCATTAC- 3` FN: FW- 5`-CACAAGATGGA TGTGTTATGG- 3`, RV- 5`-GCGTGCTGCCCAGATAAATGC- 3`; LMa5: FW- 5`-CGTACTTTAATCTAGCGGAGGGGACG- 3`, RV- GCAGTACAGGTCCTGGATA GGCTGC- 3`; LMa4: FW- 5`- GACCGTGTGCCTGCCCGCTGTC- 3`, RV- 5`-CTGGCAGACACATCTCAGAAACTC- 3`; col4a1: FW- 5`- CCTCGCAGTCTTCT TGAGCATAG- 3`, RV- 5`-CCTC ACCCTTTGCCCCTTTAAC- 3`

Dorsal Aorta Elasticity Measurement Methods

Four-day-post-fertilization larvae were anesthetized in buffered MS-222 solution and mounted in 1.5% low melting point agarose inside of a capillary tube fit with a Teflon plunger (Wheaton™ 851331) used to push the mounted larvae out of the capillary tube and into the light sheet. A region of interest of 300 X 150 microns centered on the dorsal aorta above the yolk sac extension was selected for imaging. Restricting the size of the imaging area increased acquisition speed to 22 frames per second. Movies were quantified and processed using Volocity Software (PerkinElmer, Inc.) and ImageJ and the movie montages were assembled using iMovie 10.1.1 and 9.0.4 (Apple Inc.). Data was generated by measuring the maximal aortic width and minimal aortic width at three locations and at three time points per fish. The following equation was utilized to

generate a percent diameter change: [(max width-min width)/min width]*100. The data is presented as an average of data from 4-6 fish with a minimum of 3 measurement regions per individual fish made ± s.e.m.

Kaede Photoconversion

Zebrafish carrying the Tg(*Ola-Twist:gal4*)^{sq11}; Tg(*UAS:kaede*)^{rk8} constructs were laterally mounted in 1.0% LMP agarose at 4 dpf. A region of interest (ROI) and Z-stack through the embryo was set, and 405 nm blue laser light was focused on the ROI for approximately 10 min (the duration of time it took to acquire the Z-stack). A second stack utilizing the green 488 nm and red 561 nm lasers was acquired to insure complete conversion of the kaede protein. Representative images were then acquired from within the photoconverted ROI for analysis at 4 dpf.